

Geological Society of America Bulletin

Distribution and provenance of the middle Miocene Eagle Mountain Formation, and implications for regional kinematic analysis of the Basin and Range province

Nathan A. Niemi, Brian P. Wernicke, Robert J. Brady, Jason B. Saleeby and George C. Dunne

Geological Society of America Bulletin 2001;113;419-442
doi: 10.1130/0016-7606(2001)113<0419:DAPOTM>2.0.CO;2

Email alerting services click www.gsapubs.org/cgi/alerts to receive free e-mail alerts when new articles cite this article

Subscribe click www.gsapubs.org/subscriptions/ to subscribe to Geological Society of America Bulletin

Permission request click <http://www.geosociety.org/pubs/copyrt.htm#gsa> to contact GSA

Copyright not claimed on content prepared wholly by U.S. government employees within scope of their employment. Individual scientists are hereby granted permission, without fees or further requests to GSA, to use a single figure, a single table, and/or a brief paragraph of text in subsequent works and to make unlimited copies of items in GSA's journals for noncommercial use in classrooms to further education and science. This file may not be posted to any Web site, but authors may post the abstracts only of their articles on their own or their organization's Web site providing the posting includes a reference to the article's full citation. GSA provides this and other forums for the presentation of diverse opinions and positions by scientists worldwide, regardless of their race, citizenship, gender, religion, or political viewpoint. Opinions presented in this publication do not reflect official positions of the Society.

Notes

Distribution and provenance of the middle Miocene Eagle Mountain Formation, and implications for regional kinematic analysis of the Basin and Range province

Nathan A. Niemi*
Brian P. Wernicke
Robert J. Brady
Jason B. Saleeby

Division of Geological and Planetary Sciences, California Institute of Technology, 1200 East California Boulevard, Pasadena, California 91125, USA

George C. Dunne

Department of Geological Sciences, California State University, 18111 Nordhoff Street, Northridge, California 91330, USA

ABSTRACT

Conglomeratic strata from middle Miocene sections in the central Resting Spring Range and nearby Eagle Mountain, California, contain a clast assemblage including marble, orthoquartzite, fusulinid grainstone, and coarse (~1 m) monzogabbro, interstratified with tephra yielding laser-fusion $^{40}\text{Ar}/^{39}\text{Ar}$ ages of 11.6, 13.4, and 15.0 Ma. Petrographic and geochronologic evidence ties the clast assemblage to a source area in the southern Cottonwood Mountains, California, >100 km west-northwest of their present location. In the upper 100 m of the Resting Spring Range section, conglomerates are derived almost exclusively from the southern Cottonwoods source, and sandstone modes are as much as 50% angular plagioclase derived from the monzogabbro. The lack of dilution of this detritus by other sources and sedimentary features in both sections indicate (1) that deposition occurred on an alluvial fan with a north-northeast paleoslope and (2) that transport of the gravels by sedimentary processes was probably <20 km north-northeast, in a direction normal to the present azimuth to their source. Therefore, we interpret most or all of the net east-southeast transport as a result of extensional and strike-slip faulting between the Cottonwood Mountains and the Resting Spring Range since 11–12

Ma. Restoration of these deposits to a position 10–20 km north-northeast of the eastern margin of the monzogabbro source (east margin of the Hunter Mountain batholith) yields a net tectonic displacement of the Cottonwood Mountains relative to the Resting Spring Range of 104 km N67°W. This result confirms previous reconstructions based on the restoration of isopachs in the Cordilleran miogeocline, pre-Cenozoic structural features, and other proximal Tertiary deposits in the region.

Keywords: clastic rocks, Death Valley, extension, Miocene, provenance, sedimentary basins.

INTRODUCTION

Evolving debate over the magnitude, style, and timing of Cenozoic extensional tectonics in the Basin and Range province centers on the identification, correlation, and reconstruction of preextensional markers, such as isopachs, facies trends, thrust faults, and paleo-isothermal surfaces (e.g., Snow, 1992). The extreme extension suggested by many of these reconstructions is a starting assumption for physical models bearing on the bulk constitutive properties of the deep continental crust (e.g., Kruse et al., 1991; Wdowinski and Axen, 1992). In addition, a large fraction of Pacific–North America plate motion is absorbed within the Basin and Range, and therefore regional kinematic analysis is fundamen-

tal to the problem of how plate motion influences continental deformation (e.g., Atwater and Stock, 1998; Wernicke and Snow, 1998). This type of analysis is particularly germane to the central Basin and Range (near the latitude of Las Vegas; Wernicke, 1992), where determination of the Neogene motion of the Sierran–Great Valley subplate relative to the Colorado Plateau is possible via reconstruction of a wealth of stratigraphic and structural markers spanning the entire province (Wernicke et al., 1988; Dickinson and Wernicke, 1997).

One reconstruction of such an array of regional markers in the central Basin and Range suggests 250 km of west-northwest motion of the southern Sierra Nevada relative to the Colorado Plateau since ca. 16 Ma (Wernicke et al., 1988; Snow, 1992). The largest proposed offset of a specific geologic feature in that reconstruction, and to our knowledge, anywhere in the Basin and Range, is based on the correlation of the Panamint thrust at Tucki Mountain with the Chicago Pass thrust in the Nopah–Resting Spring Range area, indicating about 92 km of west-northwest separation of the two ranges (Fig. 1). The Panamint–Chicago Pass correlation (Wernicke et al., 1988, 1993) was initially implied by Stewart's (1983) reconstruction of isopachs and facies trends of pre-Mesozoic formations in the region, which closely juxtaposed Tucki Mountain and the Resting Spring Range. This reconstruction was later supported by correlations of a suite of three contractile structures

*E-mail: niemi@gps.caltech.edu.

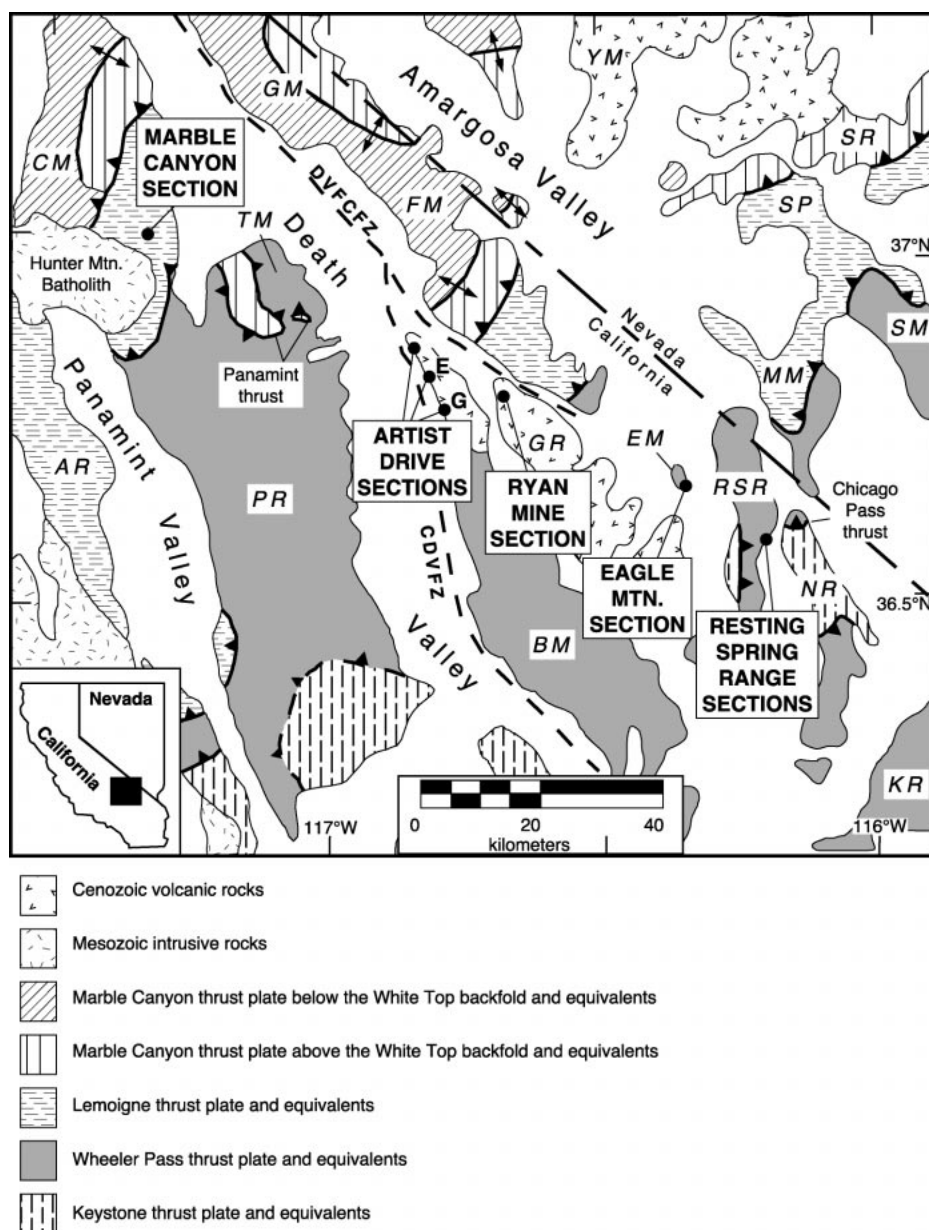


Figure 1. Map showing major ranges and basins in the Death Valley region, California and Nevada, the distribution of thrust faults and folds offset along Cenozoic normal and strike-slip faults, the Hunter Mountain batholith, and the locations of selected middle and upper Miocene stratigraphic sections discussed in the text. Patterns on the range blocks indicate thrust sheets as defined by Snow (1992) and Abolins (1998), and selected Mesozoic and Cenozoic igneous rocks. Fault abbreviations: CDVFCFZ—central Death Valley fault zone, DVFCFZ—Death Valley–Furnace Creek fault zone. Mountain range abbreviations: AR—Argus Range, BM—Black Mountains, CM—Cottonwood Mountains, EM—Eagle Mountain, FM—Funeral Mountains, GM—Grapevine Mountains, GR—Greenwater Range, KR—Kingston Range, MM—Montgomery Mountains, NR—Nopah Range, PR—Panamint Range, RSR—Resting Spring Range, SM—Spring Mountains, SP—Specter Range, SR—Spotted Range, TM—Tucki Mountain, YM—Yucca Mountain.

immediately to the west in the Cottonwood and Funeral Mountains, respectively (Fig. 1; Snow and Wernicke, 1989; Snow, 1992).

The main issues arising from these studies are (1) the accuracy of the reconstruction based on isopachs (Prave and Wright, 1986; Snow and Prave, 1994), (2) the validity of the structural correlations (e.g., Corbett, 1990; Stevens et al., 1991, 1992; Stone and Stevens, 1993; Serpa and Pavlis, 1996), and (3) the timing of extension. The age and distribution of Neogene sedimentary rocks between Tucki Mountain and the Resting Spring Range suggest that any extreme extension across much of this area was pre-8 Ma and possibly much older (Wright et al., 1991, 1999).

Because the Tertiary strata in the region are discontinuously exposed and change facies and thickness over short distances, opportunities to use them as structural markers in large-scale reconstructions are comparatively rare. However, because of this variability, the identification of key elements in widely separated areas may help determine the geometry and kinematics of Cenozoic deformation (e.g., Reynolds and Spencer, 1985; Rowland et al., 1990; Topping, 1993). For example, in the Death Valley region, stratigraphic details of ca. 10 Ma volcanic successions in the Panamint and Black Mountains suggest at least 25 km of west-northwest extension between these two ranges since that time (Fig. 1; McKenna and Hodges, 1990). Fragments of a middle to late Miocene (ca. 12–7 Ma) basin discontinuously exposed across the southern Black Mountains area contain coarse detritus, including landslide megabreccias, apparently derived from both the northern Kingston Range and the southernmost Panamint Mountains (Fig. 1), suggesting ~70 km of separation between the two ranges since ca. 8 Ma (Topping, 1993).

Here we describe Tertiary strata that unconformably overlie Cambrian strata on the east side of the Resting Spring Range and on the southern end of Eagle Mountain. These strata are herein correlated and named the Eagle Mountain Formation (Figs. 1 and 2). These strata contain conglomerates derived in part from the Hunter Mountain area in the southern Cottonwood Mountains, more than 100 km west-northwest of Chicago Pass (Fig. 1). As elaborated below, if deposition proximal to source could be demonstrated, it would bear strongly on the isopach-based reconstruction, correlation of the Panamint and Chicago Pass thrusts, and the timing of extension.

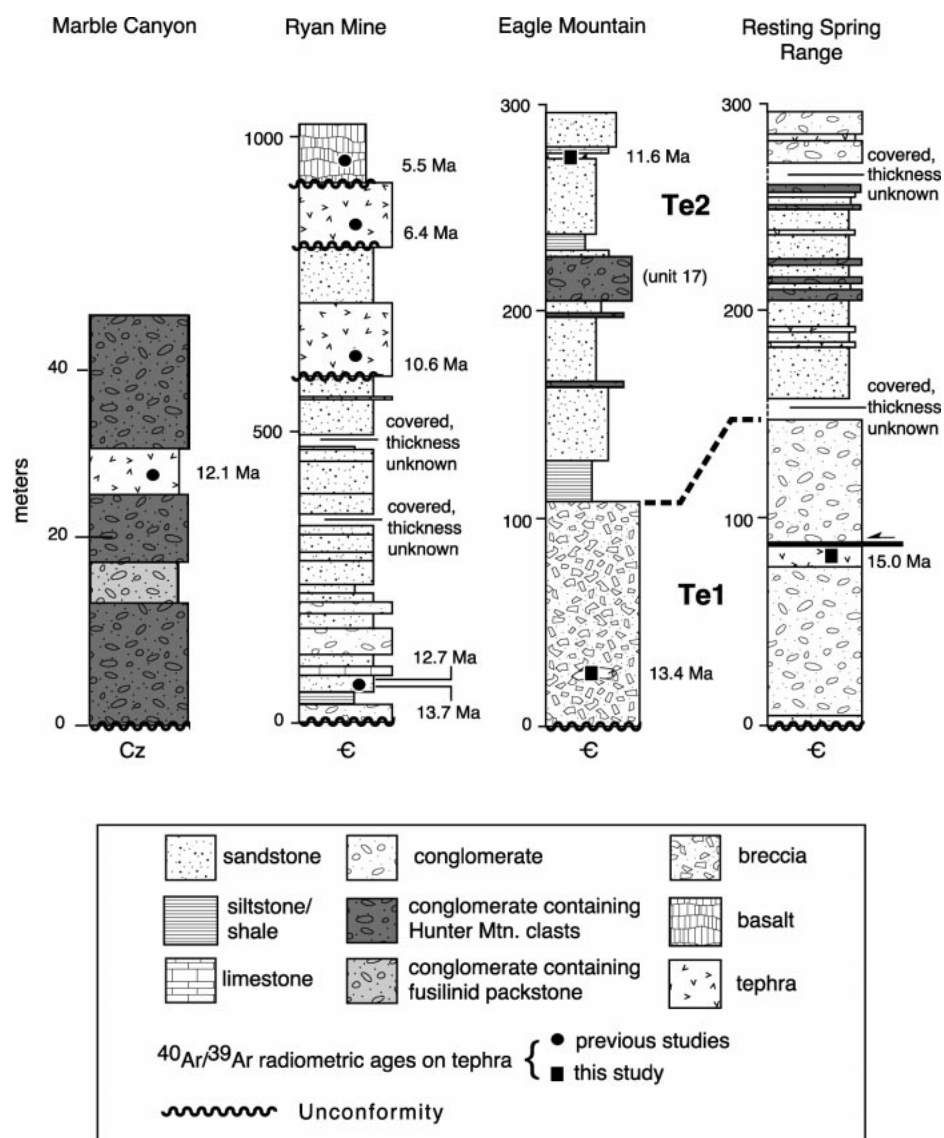


Figure 2. Columnar sections of middle and upper Miocene strata located in Figure 1, except the Artist Drive sections. Marble Canyon section is from Snow and Lux (1999). Ryan mine section is from Cemen et al. (1985) and Greene (1997). Detailed descriptions of Eagle Mountain and Resting Spring Range sections are in Appendix 1. Radiometric ages are from Cemen et al. (1985) and Greene (1997) for Ryan, Snow and Lux (1999) for Marble Canyon, and this study. Note scale differences between sections.

STRATIGRAPHIC DESCRIPTION

Eagle Mountain

Eagle Mountain is composed mainly of Cambrian miogeoclinal strata, including the Bonanza King, Carrara, Zabriskie, and Wood Canyon Formations, that dip east at $\sim 50^{\circ}$ – 60° (Stewart, 1970; Troxel, 1989). The Tertiary section is located on the southeast corner of Eagle Mountain (Fig. 1). There, the Bonanza King Formation is unconformably overlain by

~ 300 m of late Tertiary conglomerate, sandstone, siltstone, limestone, and tephra dipping $\sim 45^{\circ}$ east (Figs. 2 and 3; Appendix 1). Due to the good exposure and ease of accessibility (< 1 km north of California State Highway 127), we designate this section as the type locality of the Eagle Mountain Formation.

The section comprises two main units, a lower unit of monolithic, locally derived conglomerate and breccia, and an upper unit of mainly sandstone and conglomerate containing a wide variety of clast types that are exotic

to the local bedrock. The lower unit is 106 m thick and composed almost entirely of angular to subrounded clasts of the underlying Bonanza King Formation (Figs. 2 and 3; map unit Te1, Appendix 1, Eagle Mountain section, unit 1). It is poorly sorted, structureless, and generally clast supported. Clast imbrication was not observed. At one locality, a lens of tephra deposited within the conglomerate is present.

The 200-m-thick upper succession includes, in order of decreasing abundance, sandstone, conglomerate, siltstone, silicic tephra, and limestone (Figs. 2 and 3; map unit Te2, Appendix 1, Eagle Mountain section, units 2–32). The sandstones are feldspathic wackes that form resistant ledges (Fig. 4A) and weather a distinctive grayish-orange to moderate yellowish-brown (10YR 5–7/4). Detrital components in sandstone near the base of unit Te2 include 40% quartz; the remainder comprises subequal amounts of feldspar and carbonate lithic grains. The matrix composes 15%–20% of the rock and includes both clay and carbonate cement. The sandstones form planar beds 0.5–1 m thick. The bases of many of the sand beds are channeled (Fig. 4B), but in general individual beds can be traced laterally for tens to hundreds of meters. In the lower part of the section, below a thick conglomerate (unit 17, Fig. 2; Appendix 1), the sandstones are generally granular, whereas above the conglomerate they are finer grained. Commonly, a single sandstone bed may contain multiple horizons of angular to subrounded pebbles.

Cross-stratification in the sandstones is common but subordinate to parallel laminae. In the lower part of the section, below unit 17, local sets of 10–30-cm-thick, mostly planar, steep (10° – 30°) cross-laminae occur within conglomeratic and granular sandstones. Some of these sets terminate laterally with trough-like erosional bases into parallel-laminated sand. Above unit 17 numerous broad troughs with erosional bases are present that also contain relatively steep (10° – 30°) planar laminae. In both cross-laminated and planar-laminated sands, small-scale ripple laminae commonly occur in the uppermost parts of a given bed (Fig. 4A), and in some cases the entire bed is ripple laminated.

Massive, parallel, and locally cross-bedded conglomerate occurs throughout the section (Fig. 4, C and D), and is variably clast or matrix supported. Bedding ranges from < 1 m to 20 m thick (Fig. 4E; unit 17, Fig. 2; Appendix 1). Clasts range from angular to well rounded, and the beds are usually poorly sorted and contain a moderate to large fraction of sand

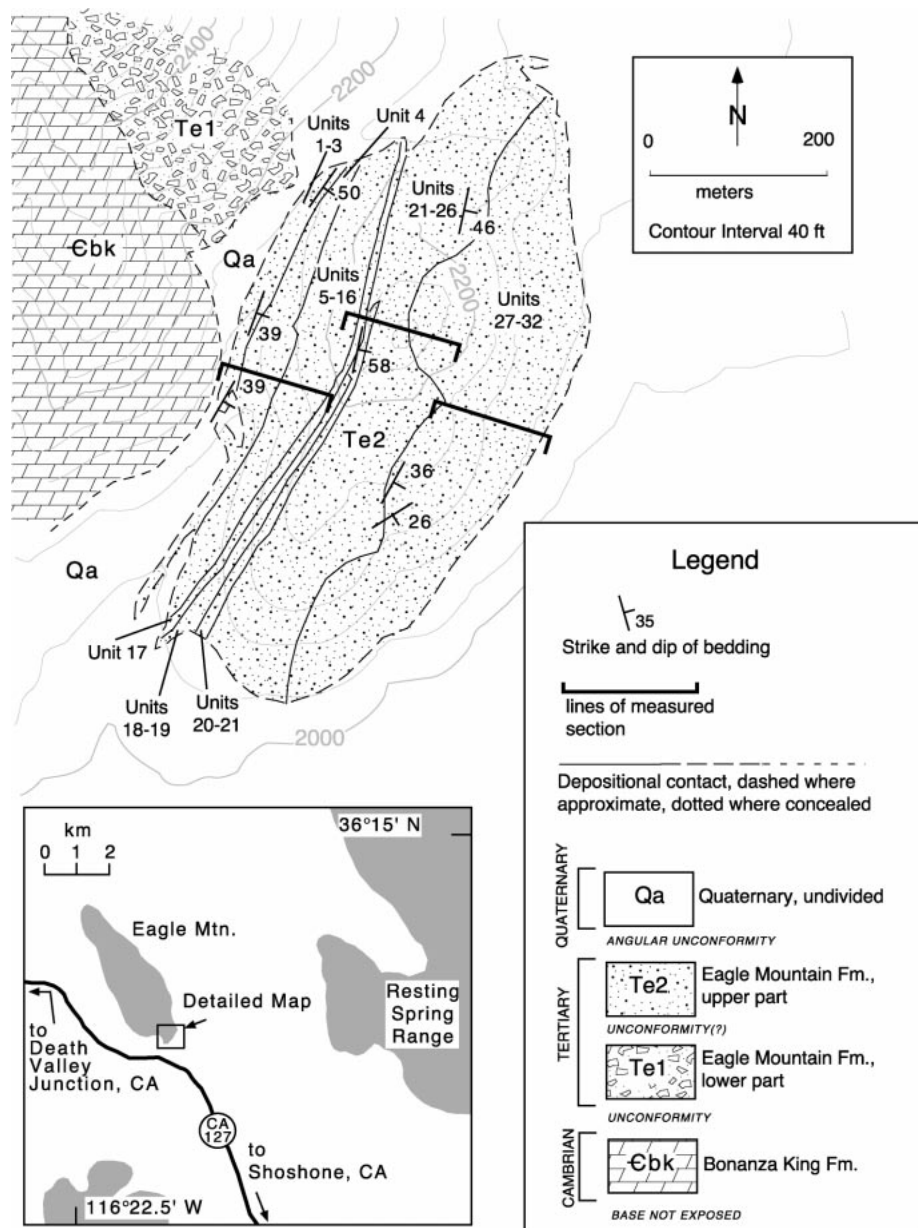


Figure 3. Geologic map of Eagle Mountain Tertiary section and location map. Geologic map shows lines of measured section. Units on geologic map correspond to those described in Appendix 1. Contour interval (40 ft) = 12 m.

(Fig. 4C). Sandy portions of the conglomerate show alternating cycles of coarse, massive to parallel-laminated sandstone and pebble and/or cobble conglomerate, each cycle being ~20–30 cm thick (Fig. 4C). The coarsest clasts are predominantly leucomonzogabbro (Fig. 4D), which have a mean clast diameter of ~15 cm; the largest clasts are >50 cm. Clast imbrication is locally present, especially near the top of conglomerate beds (Fig. 4, B and C), but in general the conglomerates are not well imbricated (Fig. 4, D and E).

Parallel-laminated siltstones (Fig. 4F) are common in the lower two-thirds of map unit Te2. A number of thin, discontinuous laminated limestones are found in the upper third.

Resting Spring Range

Moderately to steeply east dipping sandstones and conglomerates similar to those at Eagle Mountain also disconformably overlying Cambrian strata, are exposed in patches along the eastern flank of the Resting Spring Range for an

along-strike distance of at least 12 km (Burchfiel et al., 1983). They were previously referred to informally as the Chicago Valley beds (Burchfiel et al., 1982, 1983), and on the basis of the stratigraphic descriptions and radiometric ages provided below are here correlated with the Eagle Mountain Formation.

The best-exposed sections are east of Baxter Mine, where steeply east dipping Neoproterozoic and Cambrian strata are unconformably overlain by Tertiary strata that dip 50°–60° east, nearly the same as the underlying Cambrian rocks (Fig. 5). They are poorly resistant and not well exposed, except in a few isolated gullies incised through Quaternary deposits along the eastern piedmont of the range (Fig. 5). Predominant rock types, in order of decreasing abundance, are conglomerate, sandstone, limestone, silicic tephra, and siltstone (Fig. 2; Appendix 1; Wilhelms, 1962; Burchfiel et al., 1982).

In the two most complete exposures, a southern section along the Baxter Mine Road and a northern section 0.8 km to the north (Fig. 5), the sandstone and conglomerate are in depositional contact with adjacent Lower Cambrian strata, but differ markedly. The southern section (map unit Te1, Figs. 2 and 5; Appendix 1, stratigraphic units 1–4) is at least 140 m thick, and consists almost entirely of conglomerate with a prominent tephra halfway up the section. The northern section (Fig. 5; map unit Te2, Appendix 1, units 1–25) consists of 100 m of grayish-orange-weathering sandstone, pebbly sandstone, and siltstone, as well as prominent boulder conglomerate beds and several thin tephra horizons. Isolated exposures of unit Te2 to the east of unit Te1 suggest that the northern section is younger, and erosionally truncates the southern section from south to north (Fig. 5).

Basal strata of the southern section appear to be locally derived, and include clasts of Cambrian miogeoclinal clastic and carbonate strata. However, above the tephra horizon it contains a substantial percentage of younger clasts, including Ordovician orthoquartzite, Devonian limestone, and Tertiary conglomerate. Clasts are poorly sorted. The coarsest clasts in any given bed range from 20 cm (Fig. 6A) to as much as 70 cm. Rounding varies from subangular to rounded. Most of the deposit is either massive or poorly stratified, alternating between bouldery and pebbly horizons at a scale of 20–30 cm (Fig. 6A). Clast imbrication is locally observed (Fig. 6A), but not pervasive.

The northern section (Fig. 5; map unit Te2)

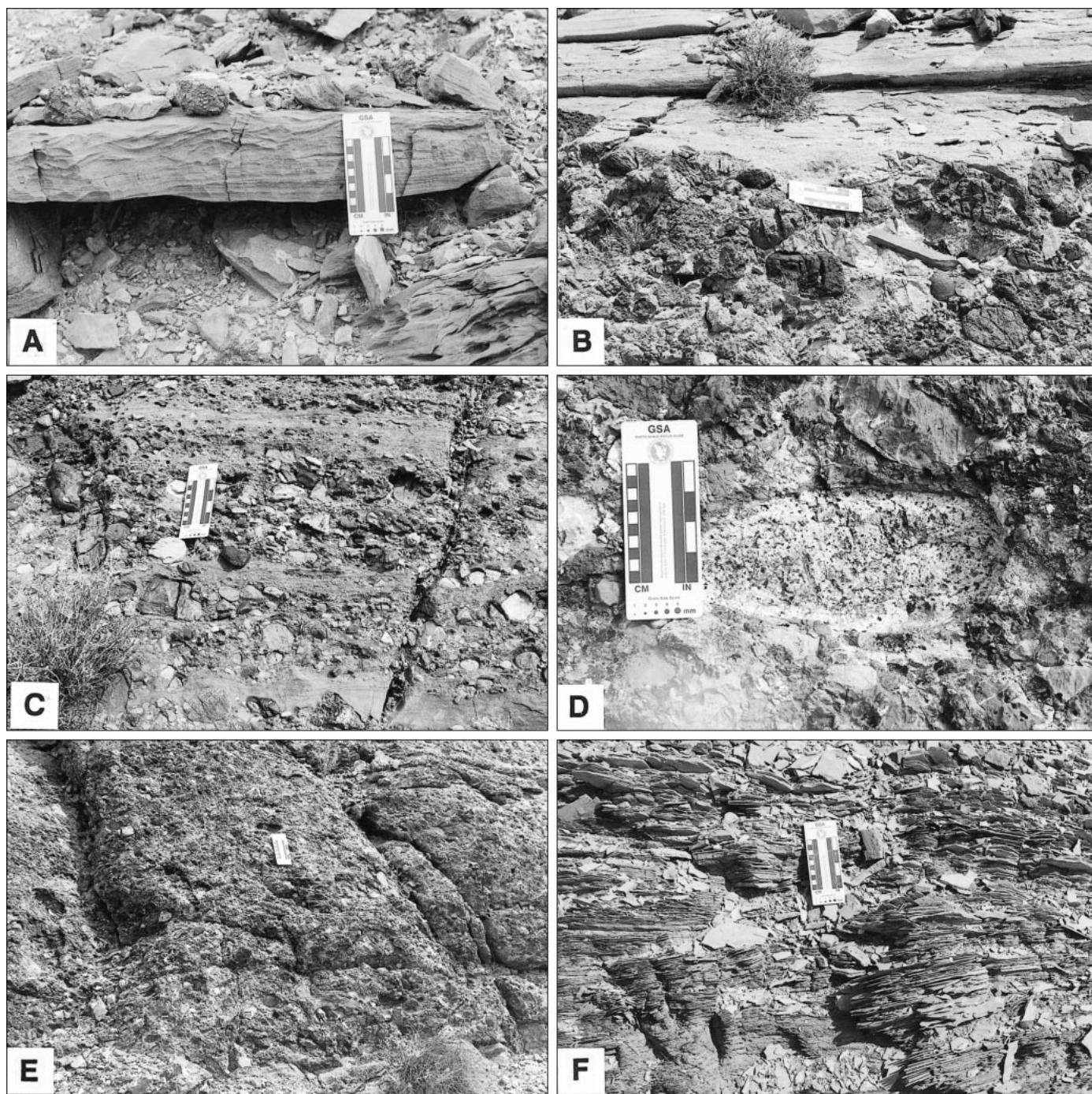


Figure 4. Eagle Mountain Formation at Eagle Mountain. Top in all photos is stratigraphic top; scale shows centimeter and inch subdivisions. (A) Typical sandstone bed at Eagle Mountain, showing low-angle cross-stratification at bottom and ripple lamination at top. (B) Base of sandstone interval above conglomerate, Eagle Mountain, showing imbricated cobbles in uppermost part of underlying conglomerate (below and right of scale) and channelization of sandstone into conglomerate. (C) Conglomerate-sandstone couplets ~20 cm thick, from unit 15, typical of sheetflood deposits on modern alluvial fans (Blair and McPherson, 1994) (D) Typical leucomonzogabbro clast, ~25 cm in maximum dimension, in a noncohesive debris-flow deposit. (E) Thick, massive conglomerate from upper part of section (unit 17). (F) Parallel-laminated siltstone, indicative, with freshwater limestones, of intermittent lacustrine conditions throughout the stratigraphic section.

TABLE 1. SUMMARY OF $^{40}\text{Ar}/^{39}\text{Ar}$ RESULTS

Sample	Location		Petrography	Mineral	Total gas age (Ma)	$^{39}\text{Ar}_p$ (%)	Isochron age (Ma)	$(^{40}\text{Ar}/^{36}\text{Ar})_0$	MSWD
	Lat ($^{\circ}\text{N}$)	Long ($^{\circ}\text{W}$)							
EM-0	36 $^{\circ}$ 11'53''	116 $^{\circ}$ 20'36''	Felsic tuff	K-feldspar	13.89 \pm 0.03	100	13.35 \pm 0.47	248 \pm 82	0.47
EM-4	36 $^{\circ}$ 11'44''	116 $^{\circ}$ 20'26''	Felsic tuff	K-feldspar	12.12 \pm 0.02	99	11.63 \pm 0.32	281 \pm 87	0.53
1593*	36 $^{\circ}$ 06'07''	116 $^{\circ}$ 12'43''	Felsic tuff	K-feldspar	21.53 \pm 0.04	100	15.04 \pm 0.24	299 \pm 89	1.33
1893†	36 $^{\circ}$ 06'33''	116 $^{\circ}$ 11'57''	Felsic tuff	K-feldspar	165.72 \pm 1.50 [§]				
1893‡	36 $^{\circ}$ 06'33''	116 $^{\circ}$ 11'57''	Felsic tuff	K-feldspar	81.99 \pm 0.68 [§]				

Notes: For each sample, our interpretation of the best apparent age is the isochron age. Entries in the total gas age column were calculated following the method outlined by McDougall and Harrison (1988). The percentage of the total ^{39}Ar in a given sample that was released in the heating steps included in the plateau is shown in the column labeled $^{39}\text{Ar}_p$. Isochron ages were calculated from laser fusion data using least-squares linear regression with correlated errors (York, 1969). $(^{40}\text{Ar}/^{36}\text{Ar})_0$ indicates the initial value for each sample. The MSWD (mean squared weighted deviation) is shown for all regressions. Analytical data are available as Data Repository Tables DR-1 to DR-13 (see text footnote 1 on p. 427).

*For sample 1593, the model total gas age is based on an assumed $(^{40}\text{Ar}/^{36}\text{Ar})_0$ of 295.5. This assumption may be invalid, based on the $(^{40}\text{Ar}/^{36}\text{Ar})_0$ measured for 10 laser fusion increments on the same sample (Table DR-8; see text footnote 1), which indicate excess ^{40}Ar . This excess ^{40}Ar may account for the discrepancy between the total gas and isochron model ages of sample 1593. See Figure 9 and text for further discussion. Inverse isochron analysis of sample 1593 (Fig. 9) identifies two isochrons of the same age, within uncertainty. The first isochron has an $(^{40}\text{Ar}/^{36}\text{Ar})_0$ of 299 \pm 89, the second has an $(^{40}\text{Ar}/^{36}\text{Ar})_0$ of 1900 \pm 954. The best apparent age was interpreted to be the isochron with an $(^{40}\text{Ar}/^{36}\text{Ar})_0$ of 299. See text for further discussion.

†Samples 1893A and 1893B relate only to the provenance of the Eagle Mountain and not to its age, hence a less comprehensive geochronological analysis was performed on these samples than on EM-0, EM-4, and 1593.

‡Age given is ^{39}Ar weighted mean age.

includes a lower, sand-rich part (stratigraphic units 1–10, Appendix 1) about 30 m thick, and an upper part containing boulder conglomerates. Throughout the northern section, sandstones form ledges 0.5–2.0 m thick, and weather a distinctive grayish-orange to pale yellowish-orange (10YR 7/4 to 10YR 8/6). They are medium- to coarse-grained, angular to subrounded, feldspathic wackes, commonly containing subangular to subrounded pebbles. Detrital components from unit 2 (Appendix 1) include 50% angular plagioclase and 25% each quartz and carbonate grains (Fig. 6B). The matrix comprises 15%–25% of the rock, and contains both clay and carbonate cement. Bedding is generally either massive or parallel laminated, and includes ripple laminae near the tops of some beds. In the lower part, pebbles are derived from the local bedrock. Although the area of outcrop is not large enough to determine the lateral persistence of individual sand beds for more than 10–20 m, no terminations or truncations of individual beds were observed.

At about 46 m up from the base of the section, a bed of very coarse boulder conglomerate and four higher coarse-boulder beds are composed of abundant monzogabbro and other clast types exotic to the local bedrock and devoid of Cambrian clasts. Clasts generally range from 30 to 70 cm in diameter, but are locally >1 m in maximum dimension (Fig. 6C). The conglomerates are clast supported, poorly sorted, contain a substantial portion of sand, and are generally more rounded than those in the southern section (subrounded to well rounded, versus subangular to rounded). Limestones and tephra (e.g., Fig. 6D) are found throughout the section.

DEPOSITIONAL ENVIRONMENT AND FACIES ASSOCIATIONS

Eagle Mountain

We interpret the Eagle Mountain Formation at the type locality to be divisible into six main facies: (1) massive, locally derived conglomerate and breccia; (2) thick, sand-rich, massively bedded pebble to boulder conglomerate (Fig. 4, B, D, and E); (3) parallel-bedded granular sandstone and conglomerate (Fig. 4C); (4) planar and cross-bedded sandstone and pebbly sandstone (Fig. 4A); (5) parallel-laminated siltstone and fine sandstone (Fig. 4F); and (6) limestone. We infer depositional environments by examining each facies and their possible associations.

The conglomerate and breccia facies composes unit Te1 (Fig. 3). On the basis of the angularity of clasts, local provenance, lack of bedding, and lack of matrix we interpret these as rock avalanche deposits.

The massive conglomerate facies occurs in the lower part of unit Te2 (Fig. 3), and is predominantly clast-supported pebble to boulder conglomerate. We interpret these deposits as noncohesive debris flows (e.g., Blair and McPherson, 1994), on the basis of the lateral continuity of individual units, coarseness, poor sorting, thick, massive bedding, angularity of clasts, and lack of a clay-rich matrix.

The granular sandstone and conglomerate facies also occurs in the lower part of unit Te2, and consists of vertically alternating pebble to cobble conglomerate and granular sandstone. On the basis of the regularity of the vertical cycles, thickness of each cycle in the 20 cm range, grain size alternating between granular

sand and pebble to cobble gravel, parallel bedding, and unimodal upper flow regime sedimentary structures (discussed below), we interpret these deposits as sheetflood couplets (cf. Fig. 4C with Fig. 11A of Blair, 1987, or with Fig. 18, A–E, of Blair and McPherson, 1994).

The sandstone and pebbly sandstone facies occurs as relatively gravelly deposits below unit 17, and as predominantly sandy deposits above. We interpret this facies as either a sandskirt facies of sheetflood deposits, or as relatively tabular fluvial braidplain deposits, on the basis of lateral continuity of bedding, alternation between pebbly sandstone and sandstone deposition within individual beds, and planar and trough cross-bedding. On the basis of paleoflow directions, the lower deposits are most likely the former, and the upper deposits the latter (see below).

The siltstone and fine sandstone facies occurs as a relatively thick unit at the bottom of unit Te2 (Fig. 3) and as a relatively thin horizon about two-thirds of the way upsection. On the basis of fine grain size, lack of mudcracks or evaporitic horizons, and a lack of current-derived sedimentary structures, we interpret this facies as lacustrine.

The limestone facies occurs in a number of thin, discontinuous beds in the uppermost part of the section. The limestones are micrites with algal laminae, and locally contain lenses of rippled fine sandstone. A lack of mud and organic material, as might be expected in a paludal environment, suggests that they are lacustrine.

The association of facies 1–3 suggests that most of the Eagle Mountain Formation was deposited on an alluvial fan (e.g., Rust and Koster, 1984; Blair and McPherson, 1994;

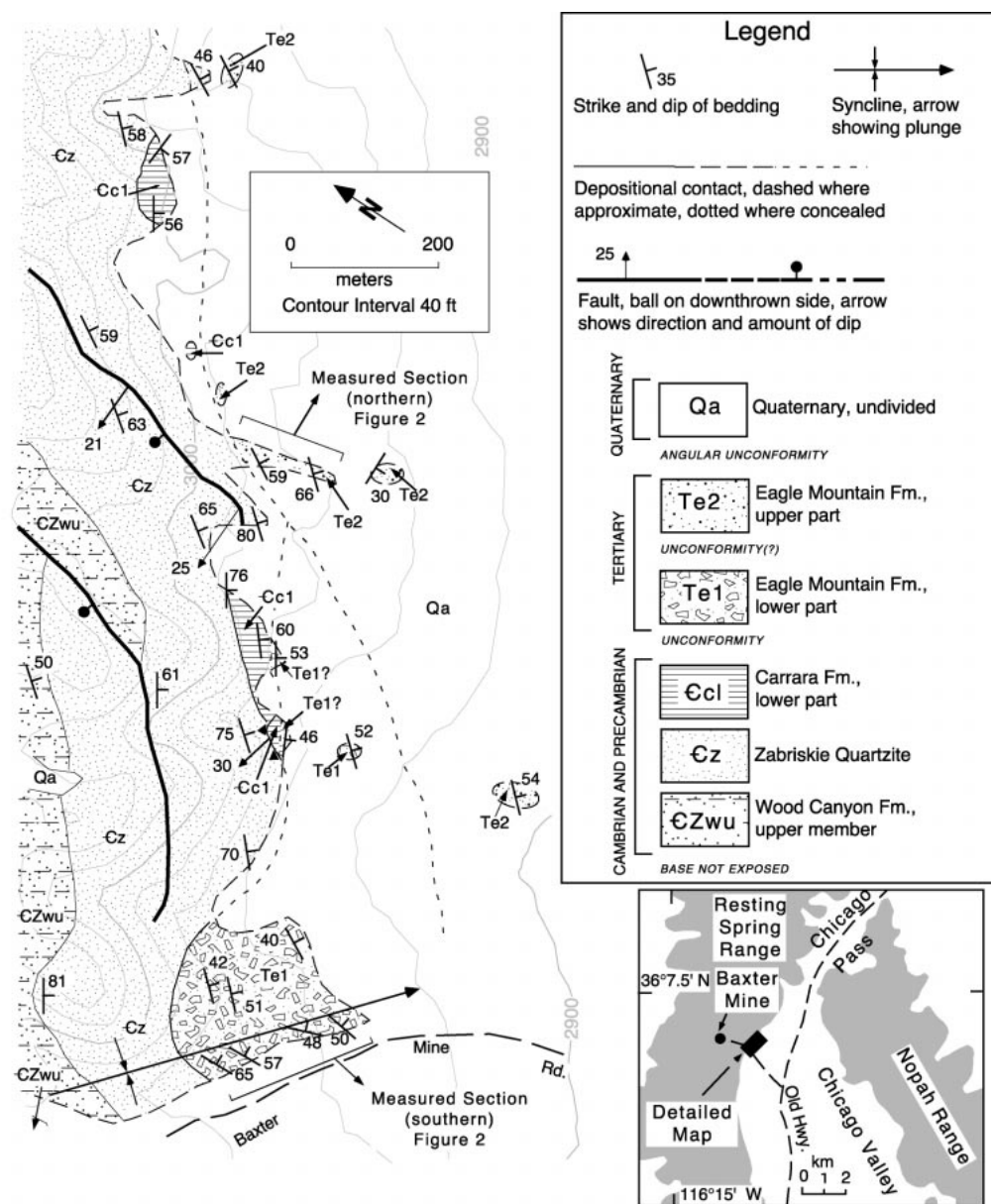


Figure 5. Geologic map of a portion of the eastern Resting Spring Range east of Baxter Mine, showing Tertiary deposits and underlying bedrock. Descriptions of Tertiary sections are in Appendix 1. Lines of measured section are shown. Contour interval (40 ft) = 12 m.

Dorsey and Roberts, 1996). The upward progression from rockfall and/or rockslide to debris flow, sheetflood, and sandskirt facies is consistent with a depositional system that evolved from a relatively small drainage area to a larger one, and is consistent with upward change in clast derivation from local bedrock to a more distal source. Facies 4 is more likely the result of braidplain deposition by ephemeral streams. This facies may represent a transition from locally derived rock avalanche and alluvial fan deposits to more distally derived alluvial fan or fluvial deposits as the local drainage basin was integrated into a larger and

more organized depositional system. That the siltstone and limestone facies occur throughout the upper part of the section suggests that the depositional system fed into a lake for much of its later history.

Resting Spring Range

The facies associations in the Resting Spring Range are less well defined than those at Eagle Mountain, owing to the relatively limited outcrop. Overall, the rock types in the two sections are similar, and the progression from a locally derived conglomerate to a sand-

rich succession containing a similar set of exotic clasts is well defined in both areas. However, the facies within each of these subdivisions differ, as might be expected. We recognize five principal facies in the Resting Spring Range, including (1) locally derived conglomerate (Fig. 6A), (2) sandstone and pebbly sandstone (Fig. 6B), (3) leucomonzogabbro conglomerate (Fig. 6C); (4) laminated siltstone, and (5) limestone.

The locally derived conglomerate facies makes up the entire southern section (map unit Te1, Fig. 5), except for the tephra horizon midway upsection. In units both above and

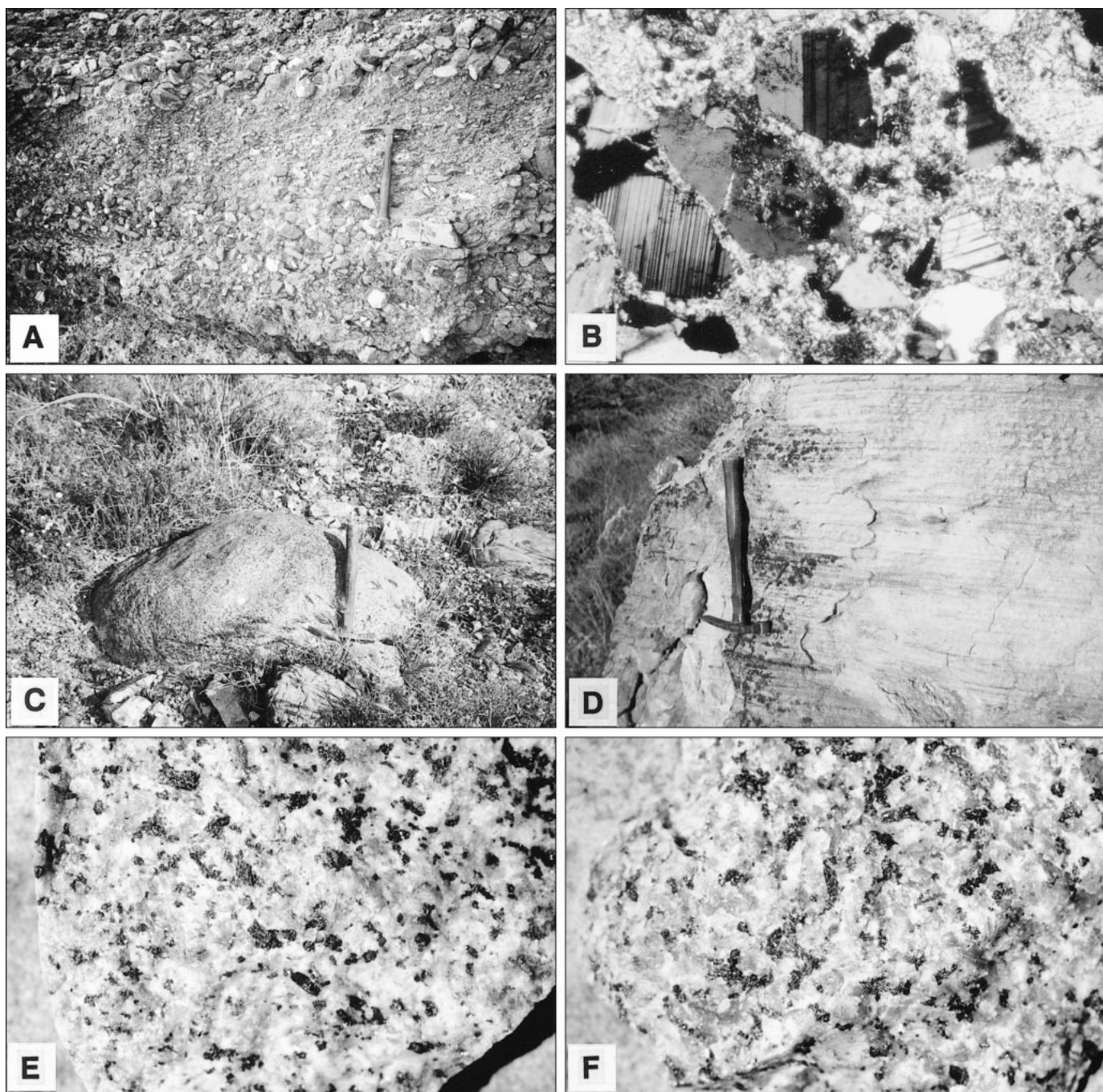


Figure 6. Eagle Mountain Formation in the Resting Spring Range. Hammer is ~30 cm long. (A) Pebble and cobble and/or boulder conglomerate couplets (unit 3 of southern section, Appendix 1). Although local imbrication of clasts is observed, this conglomerate displays no distinct beds or bedding planes and shows no consistent direction of grading. Top of photo is stratigraphic top. (B) Photomicrograph of typical arkosic wacke (sample from unit Te2, Fig. 5, in the Resting Spring Range), showing high proportions of angular plagioclase clasts. Horizontal field of view is 1 mm. (C) Lag boulder of leucomonzogabbro, >1 m in maximum dimension, in modern wash at the northern section. (D) Parallel-laminated pyroclastic fall from northernmost outcrop of unit Te2 in Figure 5, from which sample 1893 (Fig. 12) was collected. Pyroclastic fall shows no evidence of reworking. Top of photo is stratigraphic top. (E) Leucomonzogabbro clast from modern Cottonwood fan, adjacent to Hunter Mountain batholith. (F) Leucomonzogabbro clast from unit Te2 of the Eagle Mountain Formation in the Resting Spring Range. Field of view in (E) and (F) is 10 cm.

below the tephra, vertical cycles of cobbly to bouldery conglomerate and pebbly conglomerate occur in couplets 20–50 cm thick (Fig. 6A), whereas other parts of the section are massively bedded. Although the conglomerates show local imbrication, it is not a hallmark of this facies association. This characteristic and the lack of definable bedding surfaces, the gradational alternation between pebble- and boulder-size material, and the lack of sandstone or finer materials suggest deposition as either noncohesive debris flows or coarse sheetfloods.

The sandstone and pebbly sandstone facies is predominant in the northern section (map unit Te2, Fig. 5), and resembles facies association 4 at Eagle Mountain. Hence we interpret them as sandskirt deposits related to sheetflooding or fluvial deposition.

The monzogabbro conglomerate facies comprises mainly clast-supported boulder conglomerate occurring in 1–3-m-thick, massive, structureless beds with little evidence of imbrication or other internal structure. In contrast with the two conglomerate facies in the upper part of the section at Eagle Mountain, no well-defined sheetflood couplets are present (although exposure is generally not sufficient to demonstrate it). Coarse monzogabbro clasts (30–100 cm) compose approximately half the deposit, but no single bed is as thick as 20 m, as at Eagle Mountain. On the basis of the poor sorting, very coarse grain size, lack of internal structure, and clast support, we interpret these conglomerates as a result of noncohesive debris flows.

The siltstone facies occurs as thin interbeds with the sandstone and monzogabbro conglomerate facies in the middle third of the northern section. Although thin and generally not well exposed, we interpret them as lacustrine.

The limestone facies does not occur in the measured sections, but limestone beds are prominent in quarries exposed along strike a few hundred meters to the south of the southern section. They are similar to the limestones in the Eagle Mountain section, and we similarly interpret them as lacustrine.

As in the case of the Eagle Mountain section, when viewed as a whole we interpret facies 1–4 to represent deposition on an alluvial fan, and units 5 and 6 to represent deposition in an adjacent lake that existed in late Te2 time.

DEPOSITIONAL PALEOSLOPE

Although the sandstones and conglomerates throughout both sections generally exhibit

parallel or very low-angle cross-lamination and the conglomerates are generally not well imbricated, both high-angle cross-stratification and imbrication occur locally. We measured the orientations of 18 well-defined a-b plane fabrics from conglomerates in the lower and middle parts of unit Te2 on Eagle Mountain, from 18 localities evenly distributed across the area of exposure. The orientations define a unimodal population that dips to the southwest (Fig. 7A). We also measured the orientations of high-angle cross-laminae in strata assigned to facies 4, which yielded two contrasting populations. The first is recorded in the coarser sandstones below the unit 17 conglomerate. With few exceptions, they define a unimodal population with the cross-laminae dipping southwestward (Fig. 7B). The second, recorded in the finer grained sandstones above unit 17, is bimodal, one population dipping northeastward, and a slightly smaller population dipping southwestward (Fig. 7C). There is no systematic relation between stratigraphic position and the orientation of cross-laminae within the upper portion of unit Te2. Examples were observed where both dip directions were recorded in the same bed (Fig. 8A).

Paleocurrent directions in the lower portion of unit Te2 can be determined from two separate paleocurrent indicators. The south-southwest dip of imbricated clasts indicates north-northeastward paleoflow (Fig. 7A). The southwest-dipping cross-laminae in sandstones interstratified with the conglomerates are difficult to interpret as foreset laminae, because it would require oscillating depositional paleoslope in units 3–17. Cross-stratification resulting from antidune migration is generally thought to be low angle ($<10^\circ$) and difficult to preserve (e.g., Middleton, 1965; Blair and McPherson, 1994), but compelling flume-generated and natural examples of high-angle (20° – 25°) backset laminae have been described (Jopling and Richardson, 1966; Power, 1961; Hand et al., 1969). These natural examples of upstream-dipping cross-laminae generally occur in much coarser material than in flume experiments (e.g., granular sandstone and conglomerate), and share sedimentologic characteristics similar to those observed at Eagle Mountain, including coarse, wedge-shaped backset laminae that fine upward, and imbricated clasts that dip in the same direction as the backset laminae (Hand et al., 1969; cf. Fig. D in Power, 1961, with Fig. 8B). We therefore interpret the paleoflow of the lower Te2 sandstones at Eagle Mountain to be north-northeast directed.

The bimodal distribution in the upper sandstones, above the unit 17 conglomerate (Fig. 2), contrasts markedly with the lower sandstones. Because the two sets are cospatial, and in several places both orientations were observed within the same set of laminae, we interpret them as trough cross-strata. A method for determining the trough axis from bimodal trough cross-laminae (DeCelles et al., 1983) indicates that the trough axes at Eagle Mountain generally trend east-west (Fig. 7C). The trough axis plunges shallowly to the east-southeast ($\sim 3^\circ$), suggesting easterly flow, but this depends critically upon the accuracy of our rotation of the data to paleohorizontal. However, an easterly flow direction is far more likely than a westerly direction because the source region for Te2 conglomerates is to the west.

The apparent 90° change in paleoflow direction from north-northeast to east-southeast coincides stratigraphically with an overall change in depositional environment from an alluvial fan setting in Te1 and the lower part of Te2, to a braidplain setting in the upper part of Te2. Such a change would be expected as localized depocenters dominated by transverse depositional systems (fans) evolve into an integrated drainage system dominated by longitudinal transport (e.g., Bachman and Menhert, 1978; Fig. 4 in Leeder and Gawthorpe, 1987).

AGE

$^{40}\text{Ar}/^{39}\text{Ar}$ dating was attempted on seven tephra samples, four of which yielded interpretable age information (Table 1), including two samples from Eagle Mountain (EM-0 and EM-4) and two samples from the Resting Spring Range (1593 and 1893; Data Repository Tables DR1–DR13¹). Sample 1893 yielded information relevant only to the provenance of the tephra and is discussed in the next section. The stratigraphic positions of the other three samples are shown in Figure 2. Complete analytical data are listed in Tables DR2–DR10 (see footnote 1), and analytical methods are described in Appendix 2.

The results of the $^{40}\text{Ar}/^{39}\text{Ar}$ analyses are summarized in Table 1 and illustrated in Figure 9. The samples from Eagle Mountain yielded highly reproducible laser-fusion ages averaging about 13.1 Ma (EM-0, from the lower unit; Table DR2; see footnote 1) and 11.6 Ma (EM-4, near the top of the upper unit;

¹GSA Data Repository item 2001031, tables, is available on the Web at <http://www.geosociety.org/pubs/ft2001.htm>. Requests may also be sent to Documents Secretary, GSA, P.O. Box 9140, Boulder, CO 80301; e-mail: editing@geosociety.org.

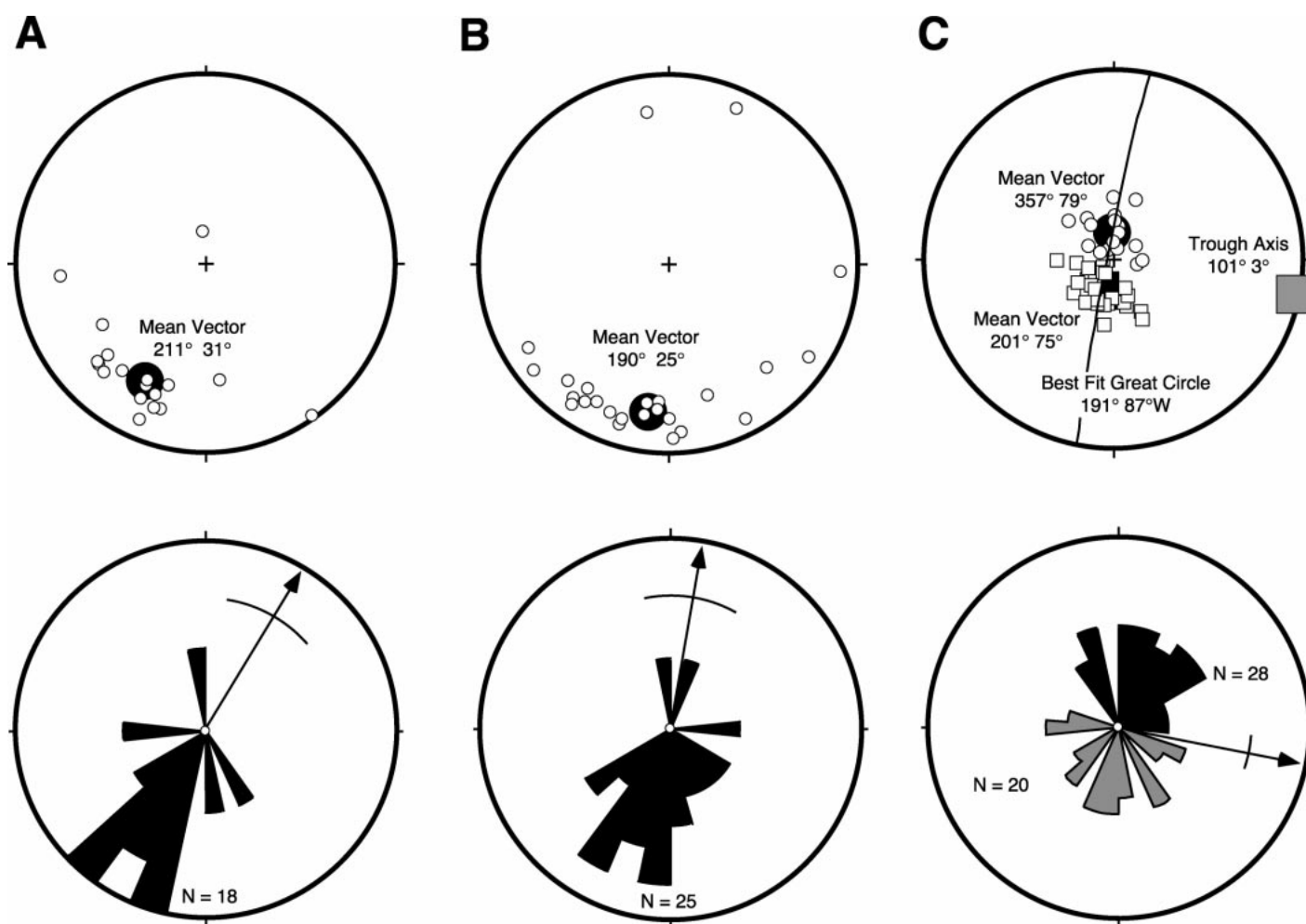


Figure 7. Orientations of paleocurrent indicators from the upper part of the Eagle Mountain Formation (unit Te2), Eagle Mountain, after backtilting local bedding to horizontal about the strike direction at each outcrop. In A and B each data set is shown as a stereographic plot of dip vectors (trend and plunge of vector raking 90°) and a rose diagram of dip directions. In C, the data set is shown as a stereographic plot of poles to cross-bedding and a rose diagram of dip directions. Large filled symbols on stereonets show mean vector of each population. N indicates number of observations. Arrows on rose diagrams indicate inferred paleocurrent direction, with arc showing 95% confidence limits. (A) a-b plane fabric in imbricated conglomerates. (B) Planar cross-laminae in granular sandstones, lower part of section. (C) Trough cross-laminae in sandstones, upper part of section, divided into northerly (circles) and southerly (squares) dipping populations. Best fit great circle is shown on the plot of poles to bedding. The pole to the best fit great circle (gray square) is interpreted as the trough axis.

Table DR5; see footnote 1). Isochron ages for these two samples are 13.4 Ma and 11.6 Ma (Fig. 9), concordant with two-step resistance furnace analyses of the bulk separates (Table 1; Tables DR3 and DR6; see footnote 1). We interpret the isochron ages as the best estimate of the eruption ages of these two samples.

Sample 1593, from the Resting Spring Range (from the middle of unit Te1), yielded slightly more scattered laser-fusion ages averaging 15.2 Ma (Table DR8; see footnote 1). Inverse isochron analysis of sample 1593 (Fig. 9) indicates that the laser-fusion increments define two distinct linear arrays, each of approximately the same age, with different initial $^{40}\text{Ar}/^{36}\text{Ar}$. The

first array yields a model isochron age of 15.04 ± 0.24 Ma with an initial $^{40}\text{Ar}/^{36}\text{Ar}$ of 299 ± 89 . The second array indicates a model isochron age of 13.58 ± 1.21 Ma, with an initial $^{40}\text{Ar}/^{36}\text{Ar}$ of 1900 ± 954 . These results suggest that sample 1593 may consist of two separate diffusion domains. The first domain consists of a mixture between a radiogenic component of ^{40}Ar and a nonradiogenic component of approximately modern atmospheric value. A mixture of the same radiogenic component as found in the first domain with a nonradiogenic component containing excess ^{40}Ar is found in the second domain.

The model total gas age of sample 1593 is

calculated to be 21.5 Ma (Table 1; Table DR9; see footnote 1). The discrepancy between model isochron and total gas ages for this sample is best attributed to the unsupported component of ^{40}Ar in the sample. The assumed initial $^{40}\text{Ar}/^{36}\text{Ar}$ used to calculate the model total gas age (295.5, the modern atmospheric value) probably underestimates the true initial $^{40}\text{Ar}/^{36}\text{Ar}$ of the bulk separate (Table 1; Fig. 9; Table DR8; see footnote 1). An initial $^{40}\text{Ar}/^{36}\text{Ar}$ in the range of 990, within the uncertainty of the measured initial $^{40}\text{Ar}/^{36}\text{Ar}$ of sample 1593 (Fig. 9; Table 1), would result in a total gas model age in agreement with the isochron age.

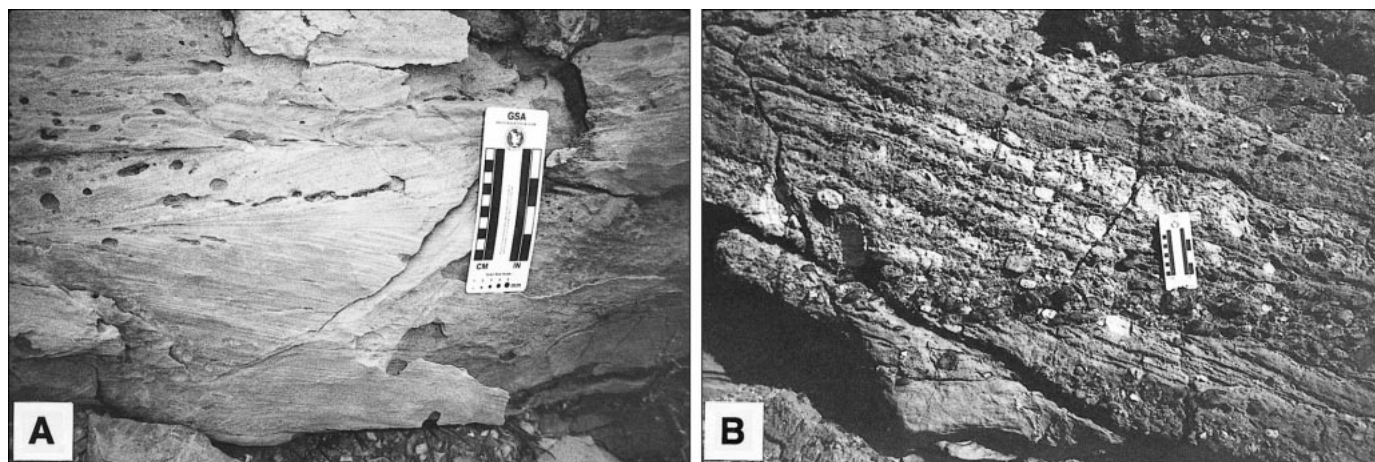


Figure 8. Cross-stratification in the Eagle Mountain Formation, Eagle Mountain. (A) Trough cross-stratification in sandstones, upper part of unit Te2. (B) Planar cross-beds in conglomerate, lower part of unit Te2. Horizontal dark gravel layer below scale is parallel to bedding. Note strong upface fining (right to left), with cobbles of light colored intraformational (?) Tertiary limestone toward the bottom fining upward to granular sand at the top, suggesting flow from right to left (northward).

Although the isochron ages for both non-radiogenic end members found in sample 1593 are equivalent within uncertainty, we have chosen the isochron age corresponding to an initial $^{40}\text{Ar}/^{36}\text{Ar}$ of 299 as the best estimate of the eruption age. We therefore interpret the age of sample 1593 to be 15.0 Ma.

A younger limit on the age of the Eagle Mountain Formation in the Resting Spring Range is provided by gently dipping ash-flow tuffs that are separated from the underlying steeply dipping Cambrian strata by an angular unconformity (Burchfiel et al., 1982). A K-Ar age of 9.6 Ma for these units was reported by Wright et al. (1991). We conclude from these data that the Eagle Mountain Formation is middle Miocene, and that deposition was relatively slow and continuous from 15 to 11 Ma.

PROVENANCE

Sedimentological Evidence

Although the lower portions of both the Resting Spring Range and Eagle Mountain sections appear to be derived from the local bedrock of the Resting Spring Range and Eagle Mountain, respectively, the upper portions of both sections contain a more diverse clast assemblage that in some cases excludes rock types from the underlying bedrock (Table 2).

The most distinctive of the exotic clasts, a coarse leucomonzogabbro, does not have a source anywhere in the eastern Death Valley region. Most of these clasts are a plagioclase porphyry containing phenocrysts 4–8 mm long in a fine-grained groundmass of anhedral

(secondary?) potassium feldspar and plagioclase with minor quartz. Mafic minerals vary in abundance from 11% to 18%, and occur in distinctive clusters of clinopyroxene and biotite, with lesser hornblende and olivine (Fig. 6F).

Other distinctive clast types found at both localities include wackestones, packstones, and grainstones composed of large (3–6 mm) fusulinids of Permian age (C.A. Stevens, 1994, oral commun.), crinoidal grainstones of probable Carboniferous age, white orthoquartzite, marble, altered intermediate (?) volcanic rocks, and gray sucrosic dolostones (Table 2). The Resting Springs Range section also contains clasts of micrite with large spiriferid brachiopods of probable Devonian age, calc-silicate hornfels, and basalt (Table 2).

The Cottonwood Mountains were recognized as a possible source terrain for these conglomerates by Wilhelms (1962, p. 117) on the basis of the occurrence of monzonitic plutons there, but he indicated that a precise locale had not been found. A specific area with the requisite characteristics to be the source region is the eastern edge of the Hunter Mountain batholith in the southern part of the Cottonwood Mountains (Figs. 1 and 10).

The interior of the batholith is a fine- to medium-grained leuco-quartz monzonite (Table 3) with an intrusive age between ca. 165 Ma (K/Ar hornblende, Burchfiel et al., 1970) and 156 Ma (K/Ar biotite and hornblende, Burchfiel et al., 1970; U/Pb zircon, J. Chen, 1997, oral commun.; Fig. 10). East of the Hunter Mountain fault zone, the batholith is

rimmed by a fine- to medium-grained monzogabbro phase dated at 175 Ma (U/Pb zircon, G. Dunne and J.D. Walker, 1997, oral commun.; Fig. 10; Table 3). The outermost rind of the batholith, best developed on the southeastern margin, is a third phase consisting of coarse leucomonzogabbro, dated at 178–180 Ma ($^{40}\text{Ar}/^{39}\text{Ar}$ biotite, J.F. Sutter, 1997, oral commun.; U/Pb baddeleyite, this report; Fig. 10; Table 3). The phase along the southeastern margin is most similar to the distinctive texture and modal mineralogy of the Eagle Mountain clasts, including porphyritic texture; plagioclase phenocrysts in the 4–8 mm range; fine-grained groundmass composed mainly of (secondary?) potassium feldspar with minor quartz; clustered mafic phases that include clinopyroxene, biotite, and olivine; and monzogabbroic modal mineralogy. Clasts of this type are abundant in Holocene fan deposits along the eastern margin of the batholith, and are indistinguishable from the clasts in the Eagle Mountain Formation (cf. Fig. 6, E and F).

The batholith is surrounded by a 1–2-km-wide contact aureole of fine- to coarse-grained marble and calc-silicate hornfels, which grade laterally away from the batholith into unmetamorphosed strata ranging in age from Ordovician to Permian. Paleozoic strata widely exposed along the northern and eastern margins of the batholith include white orthoquartzite (Eureka Quartzite) and the Permian Owens Valley Group, which is rich in fusulinid grainstone.

The combination of (1) a monzogabbroic phase of the batholith similar to leucomonzo-

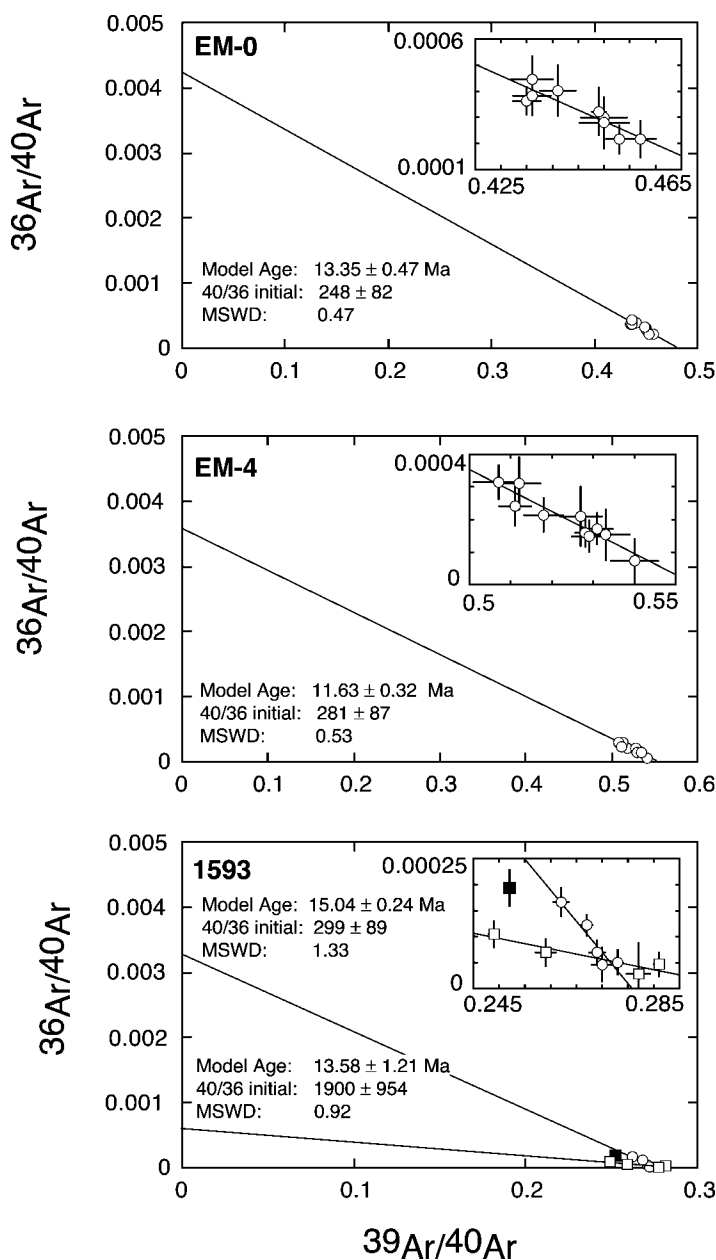


Figure 9. Inverse isochron correlation diagrams of $^{40}\text{Ar}/^{39}\text{Ar}$ data for tephros from the Eagle Mountain Formation at Eagle Mountain (EM-0 and EM-4) and in the Resting Spring Range (1593). Filled square represents a mixture of two gas components defined by unfilled symbols, and was excluded from the regression analysis (see text for discussion). Error bars are shown at 2σ where they are larger than the circle representing the point.

gabbro clasts found in the Tertiary sections; (2) a wide, largely carbonate contact aureole; (3) Ordovician through Permian miogeoclinal strata as country rock, including fusulinid grainstones; and (4) the absence of the Neoproterozoic clastic wedge, is unique to the eastern margin of the Hunter Mountain batholith in the southern Cottonwood Mountains. This area thus appears to be the only tenable exposed source area for the

clast assemblage in the upper part of the Eagle Mountain Formation in the Resting Spring Range, and for a large component of clast types in the upper part of the section at Eagle Mountain (Table 2).

An alternative source terrain could be a hypothetical region closer to Eagle Mountain that has simply been buried under the modern valleys. Such a hypothetical terrain is difficult

to rule out absolutely, but such an occurrence seems unlikely. The leucomonzogabbroic mineralogy of the Hunter Mountain batholith is distinctive, as compared to the more typical modes in the region, which are rich in quartz and potassium feldspar, and rarely contain the combination of clinopyroxene, biotite, and olivine as mafic phases. If another intrusion with mineralogy similar to the Hunter Mountain batholith existed in the Death Valley area, it would also have to share the same crystallization age, as discussed below. The intrusion would also have to share a drainage basin with abundant fusulinid grainstones. These grainstones are only abundant in Permian strata, which are omitted by the basal Tertiary unconformity in all ranges between the Panamint and Spring Mountains.

Geochronologic Evidence

The interpretation that the leucomonzogabbro clasts at Eagle Mountain and in the Resting Spring Range are from the Hunter Mountain batholith is consistent with U/Pb geochronology of the clasts and the batholith. One clast from Eagle Mountain (LMG-EM, Table 4), one clast from the Resting Spring Range (LMG-CV), and one bedrock sample from the eastern margin of the batholith in Cottonwood Canyon (LMG-CC, Fig. 10) were collected for U/Pb analysis. Sample location coordinates and analytical data are presented in Table 4 and Figure 11; analytical methods are described in Appendix 2.

The three analyses are internally concordant and appear to define a lead-loss trajectory, with discordance increasing with uranium concentration (Fig. 11; Table 4). We therefore interpret the discordance to be the result of minor lead loss due to metamictization. Although inheritance could also lead to the discordance, inheritance of baddeleyite is rare, due to its paucity in most crustal rocks. Discordance due to a prolonged thermal history is unlikely, because the U/Pb ages are similar to $^{40}\text{Ar}/^{39}\text{Ar}$ ages from the leucomonzogabbroic phase (Fig. 10). We interpret the data to indicate a crystallization of the leucomonzogabbroic phase of the Hunter Mountain batholith, and of both leucomonzogabbro clasts, ca. 180 Ma.

$^{40}\text{Ar}/^{39}\text{Ar}$ ages were determined on potassium feldspar grains from an ~2 m-thick tephra in the Eagle Mountain Formation in the Resting Spring Range (sample 1893; Tables DR11–DR13; see footnote 1). The tephra is parallel laminated throughout (Fig. 6D) and shows no evidence of reworking. In thin sec-

TABLE 2. CLAST COMPOSITION OF EAGLE MOUNTAIN FORMATION

Clast type	Resting Spring Range			Eagle Mountain Upper part Unit 17 [†] (%)	Ryan Conglomerate [§] (%)
	Upper part Location A* (%)	Upper part Unit 11 [†] (%)	Lower part Units 1 and 4 [†] (%)		
Conglomerate, sucrosic dolostone clasts	0	1	20–80	0	0
Coquina with gastropod fragments	0	1	0	0	0
Volcanic rocks (andesite, dacite, basalt)	10	1	0	1	1
Hypabyssal porphyry	0	1	0	0	0
Leucomonzogabbro, with large plagioclase phenocrysts in a quartz–K-feldspar–plagioclase matrix, clusters of hornblende, biotite, olivine, and clinopyroxene	15	50	0	5	1
Marbles and calcsilicates, hornfels	5	1	<1	7	7
Limestone, weakly recrystallized, including fusulinid wackestone and packstone and chert-limestone conglomerate	50	30	1–5	5	1
Echinodermal limestone, light to medium gray, with coarse crinoid stem debris, probably Carboniferous	0	0	10–20	1	0
Limestone, micritic, with large spiriferid brachiopods, probably uppermost Devonian	0	0	<1	0	2
White orthoquartzite, probably Ordovician Eureka Quartzite	20	15	5–10	10	41
Limestone and dolostone, dark to light gray, probably Cambrian Bonanza King Formation or Nopah Formation	0	0	0	45	35
Orthoquartzite, pinkish-gray to grayish-pink, probably Cambrian Zabriskie Quartzite	0	0	30–60	3	1
Sandstone, grayish or dusky yellow-green, probably Cambrian Wood Canyon Formation or Zabriskie Quartzite	0	0	30–80	0	0
Impure sandstone, pale purple to grayish-red-purple, probably middle member of the Wood Canyon Formation or Zabriskie Quartzite	0	0	1–5	3	0
Dolostone, yellowish-orange, locally oolitic, probably Cambrian Wood Canyon Formation	0	0	10	18	13

*Measured Section (northern) in Figure 5.

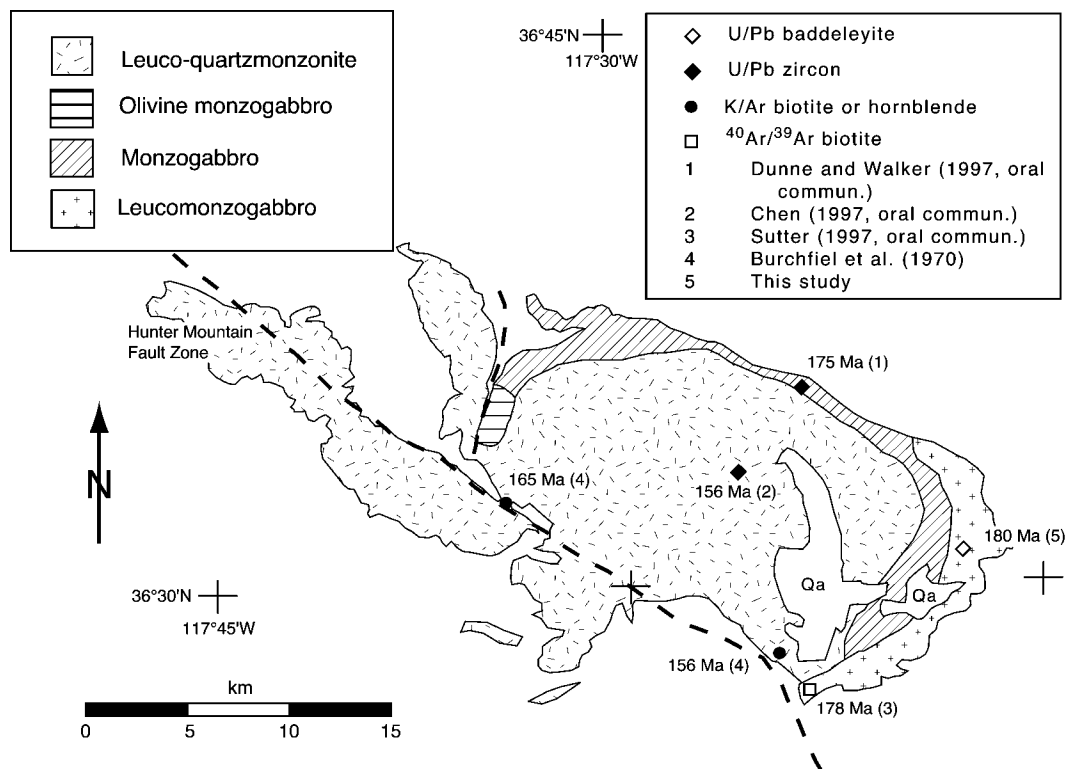
[†]Unit numbers correspond to measured sections in Appendix 1.[§]Clast composition was determined for the lower submember of the Lower Sedimentary Member of the Artists Drive Formation of Cemen and Wright (1988).

Figure 10. Geologic map of Hunter Mountain batholith, southern Cottonwood Mountains, showing distributions of plutonic phases, sample locations, and radiometric age data.

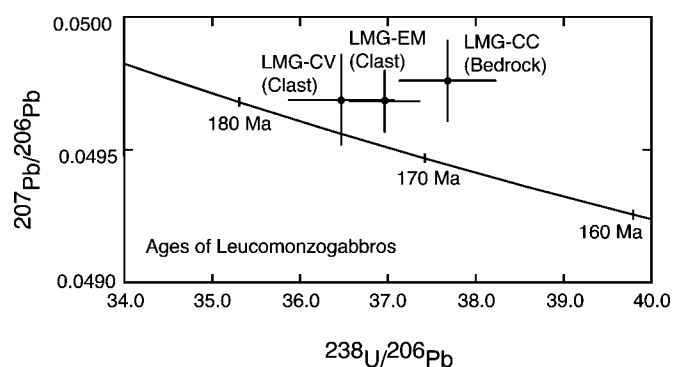


Figure 11. Concordia plot of U/Pb data (Tera and Wasserburg, 1972) of baddeleyite from leucomonzogabbros from the eastern margin of the Hunter Mountain batholith (Fig. 10) and leucomonzogabbro clasts from the Eagle Mountain Formation at Eagle Mountain and in the Resting Spring Range. Uncertainties shown are 2σ . Note internal concordance of data on the $^{207}\text{Pb}/^{206}\text{Pb}$ axis and minor dispersion along the $^{238}\text{U}/^{206}\text{Pb}$ axis, which increases with increasing U concentration (Table 4), suggesting minor lead loss due to crystal damage.

TABLE 3. MINERALOGY OF PHASES OF THE HUNTER MOUNTAIN BATHOLITH

Mineral phase	Leucomonzogabbro		Olivine monzogabbro		Monzogabbro		Leucoquartzmonzonite	
	Range	Average	Range	Average	Range	Average	Range	Average
Plagioclase (An)	41–55	47	35–66	52	55–65	58	28–55	38
K-feldspar	34–41	37	0–20	12	40–55	47	25–40	36
Quartz	0	0	0	0	5–30	15	34–56	40
Nepheline	0	0	0	0	0–6	2	5–19	14
Total mafics	11–18	16	0	0	0	0	0	0
Clinopyroxene	8–18	11	31–63	40	25–38	29	4–16	9
Biotite	3–8	4	18–33	17	15–22	17	0–5	0
Olivine	0–4	2	4–15	11	10–16	12	1–6	3
Hornblende	0	0	0–17	5	0–2	0	0	0
SiO ₂	52–53	53	0–5	1	0	0	4–15	9
Alkalies	9–10	10	44–48	46	52–59	55	58–66	62
			2–4	3	6–9	7	7–10	8

tion, ash fragments are angular and include cusped L- and C-shaped grains. Two feldspar grain populations were separated, one largely transparent, the other translucent (samples A and B, respectively), and four laser-fusion analyses were performed on each. As is typical of many of the sampled ash beds in the

Eagle Mountain Formation, the ages in sample B are spread relatively evenly between the mid-Tertiary and Middle Jurassic (38–170 Ma), but the ages from sample A are well clustered between 163 and 168 Ma (Fig. 12).

We interpret these ages as indicating that the feldspar grains were entrained by ascend-

ing Miocene magma as it passed through late Middle Jurassic plutonic or volcanic rock. Because the depositional age of the tephra is middle Miocene, possible source regions for the tephra are presumably restricted to where middle Miocene and Middle Jurassic magmatic centers coincide. Middle Jurassic plutons and volcanic rocks are not found in the eastern Death Valley region, but occur in a semicontinuous belt to the west and north of Death Valley (Saleeby and Busby-Spera, 1992). Although middle Miocene volcanism is well developed in the Nevada Test Site region, it does not coincide with the known belt of Jurassic magmatism. The closest possible source region for the tephra is in the southernmost Panamint Range. However, middle Miocene volcanism overlaps the Jurassic magmatic belt throughout much of the Mojave Desert region. Tephra that are a few meters thick can be many tens of kilometers from the source. Therefore, although suggestive of proximity to the Jurassic arc well to the west of Eagle Mountain, the Jurassic xenocryst population does not provide a precise constraint on the position of the Eagle Mountain Formation at the time of eruption.

DISCUSSION

Sedimentary versus Tectonic Transport

Our interpretations of (1) a middle Miocene depositional age, (2) a predominantly alluvial fan depositional environment, and (3) a southern Cottonwood Mountains source region for much of the detritus in the lower portion of unit Te2 at Eagle Mountain, and nearly all of unit Te2 in the Resting Spring Range, impose severe constraints on the position of the Resting Spring Range and Eagle Mountain with respect to the southern Cottonwood Mountains in middle Miocene time.

TABLE 4. BADDELEYITE ISOTOPIC AGE DATA OF LEUCOMONZOGABBROS

Sample	Location		Petrography	Amount analyzed (mg) [†]	Concentrations			Atomic ratios			Isotopic ages [§] (Ma)		
	Lat (°N)	Long (°W)			²³⁸ U (ppm)	²⁰⁶ Pb* (ppm)	²⁰⁶ Pb/ ²⁰⁴ Pb	²⁰⁶ Pb*/ ²³⁸ U	²⁰⁷ Pb*/ ²³⁵ U	²⁰⁷ Pb*/ ²⁰⁶ Pb	²⁰⁶ Pb*/ ²³⁸ U	²⁰⁷ Pb*/ ²³⁵ U	²⁰⁷ Pb*/ ²⁰⁶ Pb*
LMG-CC	36°33'51"	117°19'58"	Leucomonzogabbro	3.2	2700	62.0	49440	0.02654(38)	0.1820	0.04976(15)	169	170	184 ± 7
LMG-EM	36°11'48"	116°20'32"	Leucomonzogabbro	3.3	1867	43.8	14792	0.02705(29)	0.1852	0.04968(12)	172	173	180 ± 6
LMG-CV	36°06'17"	116°13'58"	Leucomonzogabbro	5.4	1707	40.5	16212	0.02742(44)	0.1878	0.04969(17)	174	175	180 ± 8

Radiogenic values. Radiogenic-nonradiogenic correction based on 25 picogram blank Pb (1:18.78:15.61:38.50) and initial Pb approximations: 1:18.175:15.578:38.518 (Chen and Tilton, 1991). Uncertainties in $^{206}\text{Pb}/^{238}\text{U}$ and $^{207}\text{Pb}*/^{206}\text{Pb}*$ given as (\pm) of last two digits.

[†]Fractions analyzed were separated on a Franz Isodynamic Separator at a side/front slope of 2/20 at 1.7 amps. Samples were handpicked to 99.9% purity prior to dissolution. Dissolution and chemical extraction techniques modified from Krogh (1973).

[§]Decay constants used in age calculations: $\lambda^{238}\text{U} = 1.55125 \times 10^{-10}$, $\lambda^{235}\text{U} = 9.8485 \times 10^{-10}$ (Jaffey et al., 1971). $^{238}\text{U}/^{235}\text{U}$ atomic = 137.88. Uncertainties calculated by quadratic sum of total derivatives of ^{238}U and $^{206}\text{Pb}*$ concentration and $^{207}\text{Pb}*/^{206}\text{Pb}*$ equations with error differentials defined as (1) isotopic ratio determinations from standard errors (σ/\sqrt{n}) of mass spectrometer runs plus uncertainties in fractionation corrections based on multiple runs of NBS 981, 982, 983, and U500 standards; (2) spike concentrations from range of deviations in multiple calibrations with normal solutions; (3) spike compositions from external precisions of multiple isotope ratio determinations; (4) uncertainty in natural $^{238}\text{U}/^{235}\text{U}$ from Chen and Wasserburg (1981); and (5) nonradiogenic Pb isotopic compositions from uncertainties in isotope ratio determinations of blank Pb and uncertainties in composition of initial Pb from references given above.

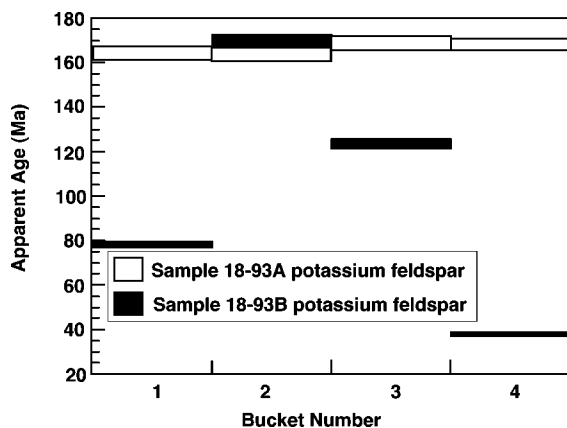


Figure 12. Plot of $^{40}\text{Ar}/^{39}\text{Ar}$ laser-fusion analyses of feldspar grains from tephra horizon in map unit Te2, Resting Spring Range (Fig. 5), shown in Figure 6D.

Empirical observations of modern alluvial fans, including their restricted radial length, exponential downstream fining of maximum clast size, and the ratio of drainage area to fan area, suggest that sedimentary transport of more than about ~ 20 km from source is unlikely. The lack of dilution from other sources of sand through boulder-sized detritus in unit Te2 in the Resting Spring Range would be es-

pecially fortuitous given the present distance from source. We therefore infer that much of the transport of the lower unit Te2 gravels away from source was tectonic.

Paleocurrent data suggest a more precise positioning of depocenter and source. Most modern alluvial fans have radii < 10 km, and radii > 20 km are virtually unknown. Studies of the depositional mechanisms on fans sug-

gest that these processes are largely ineffective at creating fan radii that exceed 10 km (e.g., Anstey, 1965, 1966; Blair and McPherson, 1994). Clasts larger than 1–2 m in diameter are uncommon more than 10 km from their source and are relatively uncommon even where found close to the source (Beaty, 1989). Downstream-fining data from modern fans compiled by Rust and Koster (1984) and Smith (1987) show that clasts with mean diameters larger than 50 cm are rarely deposited more than 10 km from source, and diameters > 1 m are rarely transported more than 5 km. Brierly et al. (1993) found that most clasts larger than 1 m were deposited within 3 km of the source. For the largest fans, the drainage area above the fan apex is roughly the same as the area of the fan, and the distance upstream from the apex to the drainage divide is generally of the same order as fan radius (e.g., Denny, 1965). Given these considerations, the Eagle Mountain fan deposits probably were just east of the southern Cottonwood Mountains during middle Miocene time (Fig. 13). The evidence for north-northeastward paleoslope in the alluvial fan deposits that compose the lower portion of unit Te2 at

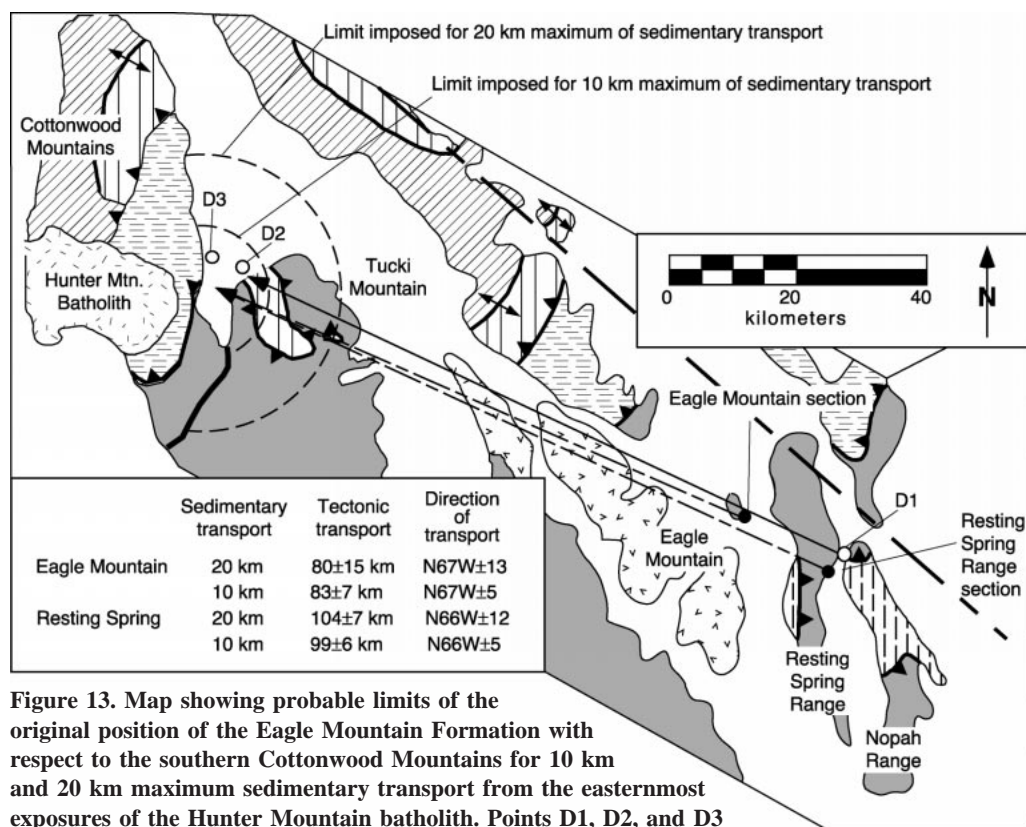


Figure 13. Map showing probable limits of the original position of the Eagle Mountain Formation with respect to the southern Cottonwood Mountains for 10 km and 20 km maximum sedimentary transport from the easternmost exposures of the Hunter Mountain batholith. Points D1, D2, and D3 are reference points in the reconstruction of Wernicke et al. (1988) discussed in text. Patterns are from Figure 1.

Eagle Mountain may suggest that a position northeast of the batholith is more likely than a position to the east or southeast. However, the precise dimensions of the ancient fan and the trajectory of streams draining the source region are unknown, so we regard a position anywhere within about 10–20 km of the eastern margin of the batholith as tenable.

As indicated by the downstream-fining data of Smith (1987), a large river system could conceivably transport meter-sized clasts many tens of kilometers from its source. The general lack of environmental indicators of fluvial deposition in the lower part of unit Te2 notwithstanding, it is difficult to envisage a drainage system 100 km long that would consistently deliver coarse detritus from the southern Cottonwood Mountains to the Resting Spring Range without contamination from other parts of the drainage system. This lack of contamination applies to the clast composition of the gravels and to the angular, plagioclase-rich arkosic wackes (Fig. 6B), both of which would be diluted by mixing with source terrains that did not include the coarse monzogabbro after only small amounts of downstream transport.

Implications for Tectonic Reconstructions

The proximity of the Cottonwood Mountains to the Resting Spring Range and Eagle Mountain ca. 12 Ma has a number of tectonic implications for the development of the central Basin and Range. It is consistent with previous reconstructions suggesting large-magnitude extension between the Panamint and Resting Spring Ranges based on correlation of pre-Tertiary features in the region (Stewart, 1983; Wernicke et al., 1988; Snow and Wernicke, 1989; Snow, 1992) and reconstructions of Tertiary basins immediately to the south (McKenna and Hodges, 1990; Topping, 1993; Davis et al., 1993).

Structural correlations of Wernicke et al. (1988, 1993) suggest juxtaposition of exposures of the Chicago Pass and related thrusts in the northern Nopah Range, where Cambrian strata are thrust over Carboniferous (Fig. 1; point D1, Fig. 13), with the corresponding stratigraphic cutoff by the Panamint thrust fault in the Tucki Mountain area (Fig. 13, point D2). In Figure 13, the cutoff along the Panamint thrust that matches point D1 must be restored northwestward to take into account extension apparent in the bedrock geology between Tucki Mountain and the southern Cottonwood Mountains, limiting the cutoff to a position between points D2 and D3 (Wernicke et al., 1988). The restored position of the Pan-

amint–Chicago Valley thrust relative to the southern Cottonwood Mountains is near the center of the region of uncertainty defined by the reconstruction of the Eagle Mountain Formation, in close accord with the previous structural correlations.

The ~100 km of post-middle Miocene separation of the Cottonwood Mountains and the Resting Spring Range leads to two testable hypotheses: (1) correlatives of the Eagle Mountain Formation may be present in the intervening area, which includes the Greenwater Range and the Black Mountains; and (2) the Greenwater Range and Black Mountains should contain a record of late Miocene (ca. 11–5 Ma) large-scale extensional tectonism, if it is assumed that the northwestward motion of the Panamint and Cottonwood Mountains occurred at a relatively constant velocity. These two hypotheses are evaluated here.

Regional Correlation of Miocene Stratigraphy

Middle Miocene strata are widespread in the Death Valley region, and on a palinspastic base occur in two major depocenters, one to the north of the Resting Spring Range and another to the south. To the north, middle Miocene sections are dominated by thick pyroclastic successions from the southwestern Nevada volcanic field in the Nevada Test Site area (Byers et al., 1976). Silicic tuffs range in age from 15.3 Ma (Redrock Valley Tuff) to 11.5 Ma (Timber Mountain Group) and have an aggregate thickness of several thousand meters (Frizzell and Shulters, 1990; Sawyer et al., 1994). The southwestern Nevada volcanic field developed at roughly the same time as rapid extension migrated westward across the region (Hoisch et al., 1997). To the south, ~3000 m of predominantly alluvial fan and lacustrine strata ranging in age from ca. 13 to 11 Ma compose the lower part of the Shadow Valley basin (Davis et al., 1993; Friedmann, 1999). The Shadow Valley basin appears to have developed in response to the onset of detachment faulting and tilting in the Kingston Range and areas to the south (Davis et al., 1993; Fowler et al., 1995; Freidman, 1999; Fowler and Calzia, 1999).

In the area between these depocenters, the middle Miocene is represented by relatively thin, predominantly epiclastic strata exposed along a northwest-trending axis extending from the central Resting Spring Range to the southern Cottonwood Mountains (Fig. 1). The four principal exposures include the two areas described in this report, the lower part of the

Artist Drive Formation as defined by McAllister (1970, 1973) in the Ryan Mine area (Cemen et al., 1985; Cemen and Wright, 1988; Wright et al., 1999), and the Entrance Narrows Member of the Navadu Formation in the central Cottonwood Mountains (Snow and Lux, 1999; Figs. 1 and 2). All of these successions appear to be quite similar in thickness, lithostratigraphy, and provenance. They contrast strongly with the middle Miocene deposits to the north and south in that they are much thinner, contain far less volcanic and volcanogenic material, and share a source region that includes the southern Cottonwood Mountains (Snow and Lux, 1999; Wright et al., 1999; this report). These successions may therefore represent an originally small, independent basin or set of basins.

Lithostratigraphy, clast composition of conglomerates, paleoslope indicators, and age of the Eagle Mountain Formation at the type locality and the lower part of the Artist Drive Formation at Ryan are all quite similar (Figs. 2 and 14). Both sections (1) unconformably overlie the Bonanza King Formation; (2) have a basal monolithic conglomerate or breccia composed of the Bonanza King Formation, giving way upward to siltstone; (3) are predominantly yellowish-brown to grayish-orange—weathering arkosic sandstones and siltstones with calcareous cement and thin limestone interbeds; and (4) contain conglomerates composed predominantly of Eocambrian and Cambrian miogeoclinal strata mixed with clasts derived from the southern Cottonwood Mountains (Wright et al., 1999). Clast-imbriation data from gravels in the lower part of the section at Ryan indicate a northward paleoslope (Fig. 4 of Cemen and Wright, 1988, p. 83), similar to the lower part of unit Te2 in the Eagle Mountain section. Cross-stratified sands above the conglomerate contain north-dipping cross-laminae (preliminary data from Wright et al., 1999, p. 103, and their Fig. 9), also in accord with our observations in the lower part of unit Te2. Tephra at the base of the section at Ryan yielded K-Ar ages of 13.7 ± 0.4 Ma and 12.7 ± 0.4 Ma (Cemen et al., 1985), well within error of the 13.4 ± 0.5 Ma $^{40}\text{Ar}/^{39}\text{Ar}$ isochron age from ash in the lower part of the section at Eagle Mountain (Fig. 14). An ash-flow tuff unconformably overlying the clastic section at Ryan yielded a K-Ar age of 10.6 ± 0.2 Ma (Cemen et al., 1985), consistent with the 11.6 ± 0.3 Ma $^{40}\text{Ar}/^{39}\text{Ar}$ isochron age from the uppermost part of the section at Eagle Mountain (Fig. 14).

On the basis of these similarities, we follow

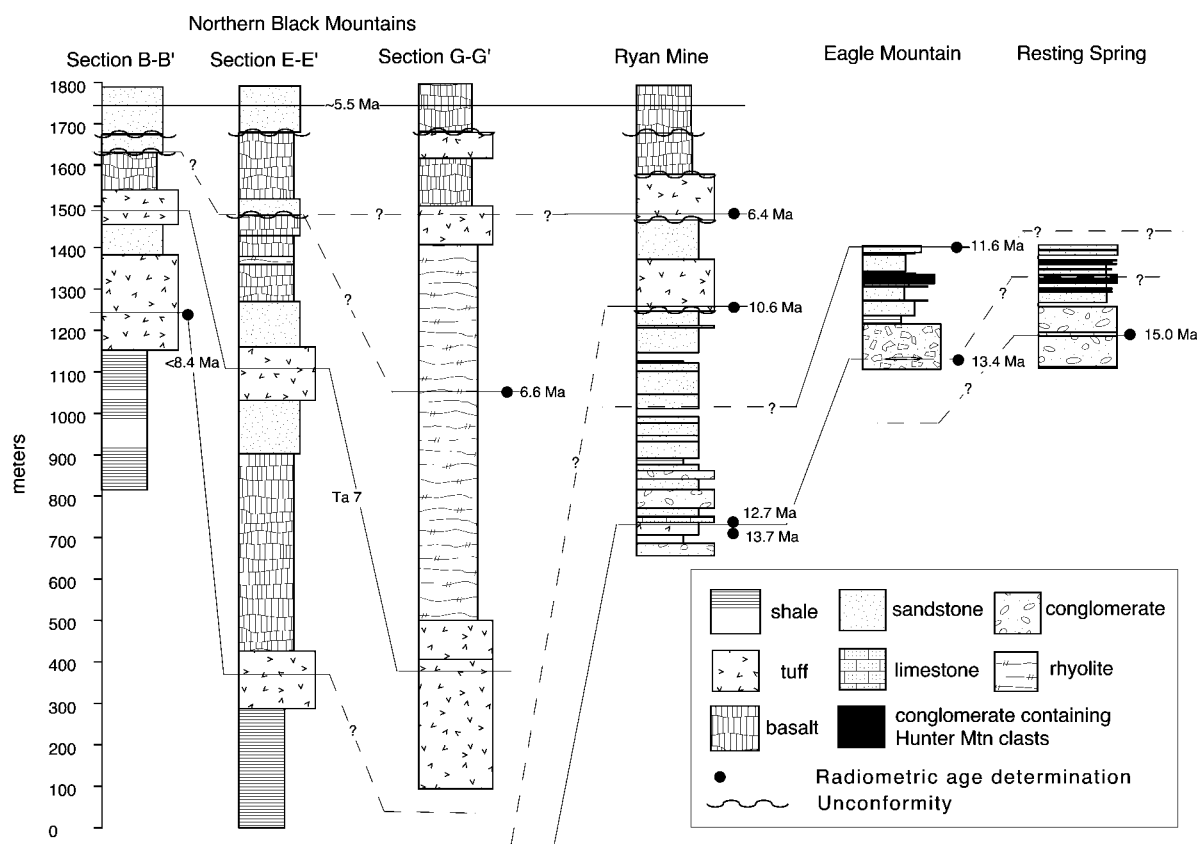


Figure 14. Correlation of sections from the northern Black Mountains, the Ryan Mine area, Eagle Mountain, and the Resting Spring Range. Section lines B-B', E-E', and G-G' are from Greene (1997); locations are shown in Figures 1 and 15. Ryan Mine section is adapted from Cemen et al. (1985), Cemen and Wright (1988), and Greene (1997).

Wright et al. (1999) and correlate the Eagle Mountain Formation with the pre-10.6 Ma siliclastic section at Ryan (unit Trs1 of Greene, 1997; lower sedimentary member of the Artist Drive Formation of McAllister, 1970). We note, however, that this section is clearly older than the oldest known strata in the type section of the Artist Drive Formation in the northern Black Mountains, which are probably younger than 8.4 ± 0.4 Ma (Greene, 1997). On this basis, Greene (1997) informally proposed the name Ryan Formation for both the Eagle Mountain correlatives near Ryan and volcanic units that unconformably overlie it. Wright et al. (1999) proposed that the section at Ryan constitute a reference section of the Artist Drive Formation, partly on the basis of correlation between lowest type Artist Drive (unit Ta1 of Greene, 1997) and the section at Ryan (unit Trs1 of Greene, 1997). As noted by both Greene (1997) and Wright et al. (1999), this correlation is tentative and awaits further geochronological work. We concur in comparison, the correlation of the pre-10.6 Ma strata at Ryan with the type Eagle Moun-

tain is now firm. We therefore designate the prevolcanic strata at Ryan as Eagle Mountain Formation, and restrict the Artist Drive designation to the volcanic-rich, post-10.6 Ma section in both areas.

This nomenclature allows unit Ta1 in the northern Black Mountains to eventually be assigned to either the Artist Drive Formation or Eagle Mountain Formation, depending on age. It also recognizes both the onset of volcanism in the central Death Valley region, and the $\sim 15^\circ$ angular unconformity between Eagle Mountain correlatives and the ca. 10.6 Ma ash-flow tuff (basal upper Miocene) at Ryan as a formational boundary (Greene, 1997, Plate 1; McAllister, 1970).

In the Cottonwood Mountains, the Entrance Narrows Member of the Navadu Formation is composed predominantly of pale yellowish-brown (10YR 7/2), grayish-orange-weathering (10YR 8/4) conglomerate with local thin interbeds of arkosic wacke, 50%–80% of the clasts being derived from the Hunter Mountain batholith (Fig. 2; Snow and Lux, 1999). An interval of monolithic breccia composed of fusulinid

grainstone from the Darwin Canyon Formation of the Owens Valley Group is also present. A tephra in the middle of the unit was dated as 12.1 ± 0.5 Ma ($^{40}\text{Ar}/^{39}\text{Ar}$ sanidine). On the basis of age and provenance we correlate the Entrance Narrows Member of the Navadu Formation with the upper part of the Eagle Mountain Formation. On the basis of their current physical separation, contrasting lithostratigraphy, and the possibility that the Navadu Formation may have been deposited in a separate basin, we suggest that the Navadu nomenclature be retained for sections now to the west of Death Valley.

The compositions of the conglomerates in the Entrance Narrows Member, now positioned just north of the Hunter Mountain pluton in Marble Canyon, are similar to those in the upper part of the Eagle Mountain Formation in the Resting Spring Range, which was derived almost exclusively from a Cottonwood Mountains source (Table 2). In contrast, unit Te2 of the type Eagle Mountain and the middle Miocene conglomerates at Ryan are predominantly from an Eocambrian–Cambrian source (Table 2). We speculate that the Entrance Narrows represents a proximal

(western or southern) facies of an alluvial fan system that fed eastward or northward into a lake. Early in the system's history, the three sections now east of Death Valley, all of which were deposited on a Cambrian substrate, were fed by a drainage area to the south underlain by Eocambrian–Cambrian strata. As the system matured, the relatively proximal Entrance Narrows and Resting Springs Range sections were fed exclusively by an expanding Cottonwood Mountains source, while the more distal-type Eagle Mountain and Ryan sections retained a southerly Eocambrian–Cambrian source that became well mixed with a component of the Cottonwood Mountains source.

Implications for the Furnace Creek Basin

The Furnace Creek basin (Cemen et al., 1985) has been defined as an ~50-km-long middle to late Miocene (ca. 14–6 Ma) depositional trough occupying the northern Black Mountains and the northern Greenwater Range (Cemen et al., 1985; Wright et al., 1999). It is delimited on the northeast by the Furnace Creek fault zone and on the west by the central Death Valley fault zone. The Furnace Creek basinal deposits interfinger southward with predominantly upper Miocene (ca. 10.5–5.0 Ma) volcanic strata of the central Death Valley volcanic field (Fig. 15; Wright et al., 1991, 1999; Greene, 1997).

Translation of the Cottonwood Mountains ~100 km northwestward away from the Resting Spring Range after 11–12 Ma implies that the area now occupied by the Furnace Creek basin was a locus of extreme extension after that time. However, Cemen et al. (1985), Cemen and Wright (1988), and Wright et al. (1991, 1999) hypothesized that deposition occurred more or less conformably throughout the preserved extent of the basin between 14 and 6 Ma, and so regard the basin as a long-lived, areally extensive depocenter. Cemen et al. (1985, p.129) suggested that because the northern Black Mountains and Greenwater Range “are now extensively underlain by an autochthonous sedimentary and volcanic cover, of which the formations of the Furnace Creek Basin are a part. . . most of the movement on the Furnace Creek segment of the [Furnace Creek] fault zone would predate the oldest basinal units.” Cemen et al. (1985) and Wright et al. (1999) favored an interpretation where northwestward translation of the basin following the onset of deposition ca. 14 Ma was no more than 10 km (Cemen et al., 1985, p. 129), and noted that this interpretation was incompatible with translation of the Panamint

Range and Cottonwood Mountains northeastward away from the Resting Spring Range and Funeral Mountains in the interval 11–5 Ma (Cemen et al., 1985, p. 128–129; Wright et al., 1999, p. 88).

In contrast, Snow and Lux (1999) interpreted the Furnace Creek basin as a synextensional to late extensional basin, the development of which was largely controlled by northwestward translation of the Cottonwood Mountains away from the Resting Spring Range between 11 and 5 Ma. Our interpretation of a proximal source in the southern Cottonwood Mountains for the Eagle Mountain Formation in the Resting Spring Range, as well as mapping by Greene (1997), support the Furnace Creek basin evolution model of Snow and Lux (1999), and refine the timing and mode of basin subsidence.

Evidence Favoring Significant Late Miocene Extension

A synextensional to late extensional origin for the Furnace Creek basin is suggested by (1) sparse preservation of middle Miocene units relative to upper Miocene units; (2) an angular unconformity between middle Miocene and younger units; (3) angular unconformities and growth-fault relations within the upper Miocene units; (4) truncation of the growth-faulted basin downward against a detachment fault; and (5) late Miocene unroofing ages of the subdetachment metamorphic infrastructure.

Following Greene (1997), we leave open the possibility that the depositional age of the oldest Tertiary unit exposed in the northern Black Mountains (unit Ta1) is ca. 8 Ma (Fig. 14). For example, unit Ta1 could be correlative with post–10.6 Ma yellowish-brown sandstones and conglomerates at Ryan (unit Trs3 of Greene, 1997). If so, then the only exposure of middle Miocene strata between Eagle Mountain and the southern Cottonwood Mountains is the section at Ryan, and possibly one additional small exposure ~5 km southeast of Ryan, previously mapped as lower Artist Drive Formation (unit Tal of McAllister, 1973). Thus, middle Miocene strata may not be coextensive with more widely exposed late upper Miocene (ca. 6–5 Ma) units that define the areal extent of the basin. A possible reason that the Eagle Mountain Formation is not coextensive with the Artist Drive Formation is that the Eagle Mountain strata may have been strongly extended in earliest late Miocene time (ca. 11–8 Ma). This inference is consistent with map relations at Ryan, indicating a 15° angular unconformity between Eagle

Mountain strata and the overlying 10.6 Ma ash-flow tuff (Greene, 1997). These strata are, in turn, in ~25° angular unconformity below ca. 4 Ma basalts (McAllister, 1970). These relations suggest that the Eagle Mountain Formation at Ryan was already a tilted fault block in earliest late Miocene time, and that tilting continued through the late Miocene (Snow and Lux, 1999).

The upper Miocene units of the Furnace Creek basin include the Artist Drive Formation (as defined below) in the Greenwater Range, and the Artist Drive and Furnace Creek Formations in the northern Black Mountains (Fig. 15). The oldest units of the Artist Drive Formation are of relatively constant thickness, and show no clear evidence of growth-fault relations (Fig. 15; units Ta1–Ta6 of Greene, 1997). Units within the middle part of the Artist Drive Formation (Fig. 15; units Ta7–Ta13), however, thicken dramatically toward the southeast (Figs. 14 and 15), and appear to have been deposited rapidly between ca. 7 and 6 Ma (Fig. 14). In addition to the southward thickening of these units, the map pattern in Figure 15 shows four prominent repetitions of the section, expressed by the geometry of marker unit Ta7, offset along three normal faults, each with map-view separations of 0.5–1.0 km. These imbricated normal faults and fault blocks are truncated by Artist Drive units Ta14–Ta30. We interpret units Ta1–Ta6 as being deposited during the early stages of an episode of extension of the basinal sediments, units Ta7–Ta13 as being deposited during extension and fragmentation of the basin, and units Ta14–Ta30 and the Furnace Creek Formation as late rift deposits that have undergone relatively little extensional fragmentation.

The thickest sections of the synextensional portions of the Artist Drive Formation (section G–G', Fig. 14) are ~1500 m thick, and are truncated downward against the Badwater turtleback fault, part of a major low-angle normal fault that served to unroof an amphibolite facies metamorphic complex in middle (?) and late Miocene time (ca. 15–5 Ma; Holm and Wernicke, 1990; Holm et al., 1992; Holm and Dokka, 1993). The thick G–G' section in the Black Mountains markedly contrasts with nearby age-equivalent strata at Ryan, which are ~200 m thick (Fig. 14). Thus, a splay of the detachment that defined the growth basin apparently was somewhere near or along the trace of the Grandview fault, which separates the Ryan Mine area and northern Black Mountains sections (Fig. 15).

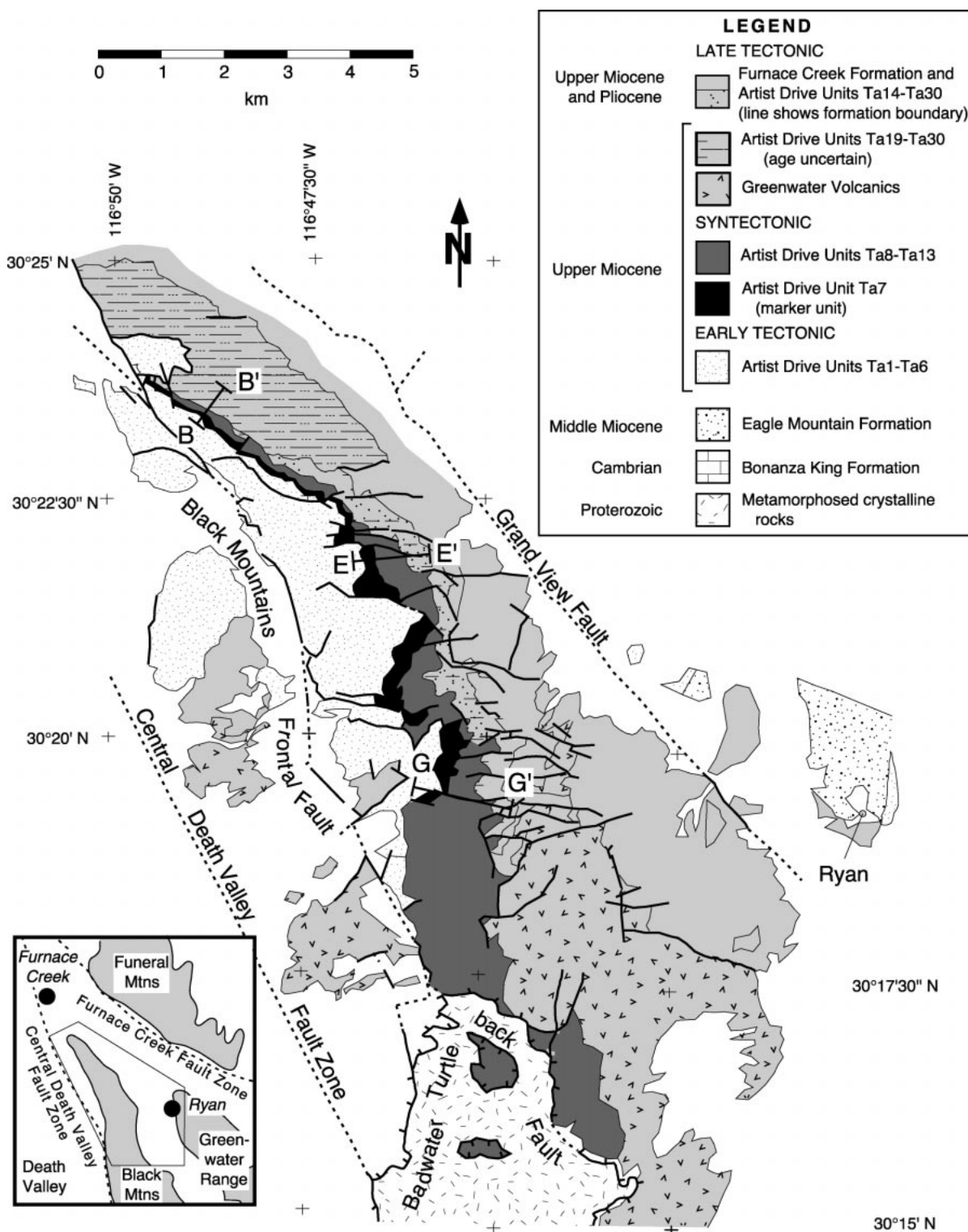


Figure 15. Generalized geologic map of northernmost Black Mountains, after Greene (1997). Designations of late tectonic, syntectonic, and early tectonic affinities of the Artist Drive Formation are based on interpretation discussed in text. Section lines refer to stratigraphic columns in Figure 14.

Interpretation

In interpreting the tectonic setting of the Furnace Creek basin, Wright et al. (1991, 1999) emphasized the apparent conformity of Eagle Mountain and Artist Drive strata from 14 to 6 Ma as problematic for models requiring major extension in the area at that time. Notwithstanding the angular unconformities and other features described here, we point out that thick, conformable sedimentation is normal in fault-proximal extensional basins during extension (e.g., Fig. 15 in Wernicke and Burchfiel, 1982; Snow and Lux, 1999). Hence we do not consider the criterion of conformability or near conformability of middle and upper Miocene strata as diagnostic of the tectonic context of the Furnace Creek basin.

Rather, following Snow and Lux (1999), we interpret these structural and stratigraphic relations to indicate that the Furnace Creek basin is a rather striking example of a supradetachment basin (see review in Friedmann and Burbank, 1995), and see little evidence in support of the hypothesis that it represents an area of tectonic quiescence in the interval 14–6 Ma.

We concur with other workers (Snow and Lux, 1999; Wright et al., 1999; Fig. 13 in Cemen et al., 1999) that, prior to Eagle Mountain deposition, the substrate of the basin was an extension-generated, erosional upland cut mainly on Cambrian strata. In early Miocene time, this upland shed detritus northward and westward onto a lowland comprising what are now the Cottonwood and Funeral Mountains, floored mainly by middle and upper Paleozoic strata. We believe that one of the structures responsible for the upland is the Tucki Wash normal fault, as described by Wernicke et al. (1993, p. 463–466).

We interpret deposition of the Eagle Mountain Formation as heralding the onset of rapid extension in the region ca. 15 Ma, which inverted the upland into a shallow early rift basin. Initial deposition of the Artist Drive Formation occurred after significant tilting and fragmentation of the Eagle Mountain strata into at least three fault blocks (Resting Spring Range, Eagle Mountain, and the northern Greenwater Range) as early as 10.6 Ma.

As the basin widened and grew westward away from the Resting Spring Range and Funeral Mountains from ca. 11 to 7 Ma, supradetachment Artist Drive deposition was for the most part conformable. From ca. 7 to 6 Ma, however, western parts of the basin internally fragmented above a shoaling detachment, imbricating units Ta1–Ta7. After 5 Ma, limited slip may have continued along the detachment

(e.g., Holm et al., 1994), but relatively intact, widespread sediments of the Furnace Creek and Funeral Formations and the cooling ages in the footwall metamorphic complex suggest that the most active segment of the detachment lay to the west.

The topographic depression created by the detachment was locally filled with as much as 2500 m of late tectonic strata from ca. 6 to 4 Ma, including units Ta14–Ta30 of the Artist Drive Formation and the Furnace Creek and Funeral Formations. Although the age control on these late extensional units is sparse, interfingering relationships of the Furnace Creek Formation southward with the Greenwater Volcanics indicate the age of the lower Furnace Creek Formation is ca. 5.5 Ma (Fig. 14; Greene, 1997). These units were tilted steeply eastward along the west flank of the range, and eroded as a result of northeast-trending shortening and coeval right-oblique normal slip on faults related to the formation of modern Death Valley from ca. 4–5 Ma to the present (e.g., Holm et al., 1994; Mancktelow and Pavlis, 1994).

Westward Migration of Tectonism and the Rolling Hinge Model

The interpretation of the development of the Furnace Creek basin described here can be integrated with other data from the region to address the question of the rolling hinge model of extensional tectonism previously hypothesized for the Death Valley region (e.g., Hamilton, 1988; Wernicke, 1992; Holm et al., 1992; Hoisch et al., 1997; Snow and Lux, 1999). One of the predictions of the model is that fault block tilting, rather than occurring synchronously as in the case of a toppling set of domino fault blocks, occurs sequentially as individual fault blocks are detached from a migrating headwall and flexurally tilted along with the abandoned fault (e.g., Wernicke and Axen, 1988; Buck, 1988; Axen and Bartley, 1997).

Deciphering any patterns in the age of tilting in the region is complicated by the fact that regional northeast-southwest compression may have resulted in steep tilts of Tertiary strata that would be unrelated to the flexural rotation process. For example, the Furnace Creek and Funeral Formations, which we interpret as having been deposited after the Cottonwood Mountains had been translated out of the northern Black Mountains area, were subsequently folded about northwest-trending axes to dips in excess of 60° and are overlain by flat-lying 4 Ma basalts (e.g., McAllister, 1970, 1973; Greene, 1997). The angular un-

conformity resulting from this folding would therefore be unrelated to any flexural rotation that may have resulted from the passage of a rolling hinge through the area.

With this caveat in mind, we recognize at least three subregions between the Nopah Range and the southern Cottonwood Mountains with contrasting ages of extension-related tilting, including (1) the Nopah–Resting Spring Range, (2) the northernmost Black Mountains and Greenwater Range, and (3) the west-central Black Mountains and the Panamint Mountains.

The Eagle Mountain Formation in the Resting Spring Range dips eastward at approximately the same angle as the underlying Cambrian bedrock, and flat-lying to gently dipping ash-flow tuffs with a reported age of 9.6 Ma unconformably overlie steeply tilted Cambrian strata (Wright et al., 1991). Therefore any flexural rotation of the range would have occurred before 9.6 Ma and after deposition of the Eagle Mountain Formation (11–12 Ma, assuming that the upper part in the Resting Spring Range is time correlative with the upper part at Eagle Mountain).

In the Greenwater Range and northernmost Black Mountains, extension-related tilting appears to have occurred mainly in the interval 9–6 Ma. Volcanic strata assigned to the Shoshone Volcanics, which range in age from ca. 7 to 8 Ma, show internal growth relations, and are generally overlain in angular unconformity by the Greenwater Volcanics and Funeral Formation basalts, which range in age from 4 to 6 Ma (Wright et al., 1991). These relations suggest that imbricate normal faulting occurred at about the same time as that observed in the Artist Drive Formation, as discussed in the previous section. These relationships are consistent with an age of 6–8 Ma for the flexural rotation of the Black Mountains based on the exhumation history of the crystalline core (Holm et al., 1992; Holm and Dokka, 1993).

In the west-central Black Mountains, the 7–3 Ma Copper Canyon Formation, which is tilted ~35°, is truncated by the turtleback fault surface (Holm et al., 1994). Along the entire western flank of the Panamint Mountains, the Miocene and Pliocene Nova Formation (ca. 6–3 Ma) is tilted eastward 15°–30° and is truncated by the Emigrant detachment, suggesting substantial unroofing of the Panamint Mountains in latest Miocene and Pliocene time (Hodges et al., 1989; Snow and Lux, 1999).

These timing constraints indicate that tilting is of middle Miocene age in the Resting Spring Range, late Miocene age in the Green-

water Range, and late Miocene–Pliocene age in the westernmost Black and Panamint Mountains, broadly consistent with a rolling hinge mechanism progressing from east to west (e.g., Snow and Lux, 1999).

The total amount of motion of ~100 km since 11–12 Ma yields an average displacement rate of 9 mm/yr. The contemporary rate of motion of the Cottonwood Mountains with respect to the eastern Death Valley region is <5 mm/yr (Bennett et al., 1997). Depending on how far back in time this rate is extrapolated, the earlier average rate becomes higher. For example, if an average maximum rate of 5 mm/yr corresponds to the development of the modern Death Valley fault zone since 5 Ma (25 km of total motion), then the average rate from 11 to 5 Ma would have been 12.5 mm/yr.

CONCLUSIONS

The middle Miocene Eagle Mountain Formation was mainly deposited on a northerly or northeasterly sloping portion of an alluvial fan, the source region of which included the southern Cottonwood Mountains. ⁴⁰Ar/³⁹Ar geochronology indicates that the Eagle Mountain Formation is older than most or all of the type Artist Drive Formation, which we herein restrict to upper Miocene strata. We interpret the Eagle Mountain Formation to be a preextensional to early extensional deposit, the current outcrop distribution of which is the result of the tectonic dismemberment of its original relatively limited areal extent.

Transport of coarse fan gravels in the lower part of the Eagle Mountain section via sedimentary processes was unlikely to have exceeded 20 km. Because the paleoslope direction of the fan is orthogonal to the transport direction, the amount of tectonic motion is insensitive to the hypothesized fan radius. If the Resting Spring Range section originally occupied a position 10–20 km north-northeast of the eastern margin of the southern Cottonwoods source region, most or all of the current separation between the eastern flank of the southern Cottonwood Mountains and the section in the Resting Spring Range (~104 km, oriented N67°W) is tectonic.

This conclusion is consistent with previous reconstructions based on isopachs and structural markers, and with the timing and amount of offset of Tertiary basins in the southern Death Valley region. In addition, it indicates that the two ranges were adjacent to one another until 11–12 Ma. The locus of extension traced a path from the southeast to the northwest at an average rate of ~9 mm/yr, which, in light of the much slower rate of contemporary

deformation, was probably substantially higher during the early phases of displacement.

APPENDIX 1. MEASURED SECTIONS

Tables A1–A3 contain measured sections of the Eagle Mountain Formation, including the type section at Eagle Mountain, and the southern and northern sections in the Resting Spring Range, all in California.

TABLE A1. EAGLE FORMATION TYPE SECTION

Bed	Description	m
Southeastern corner of Eagle Mountain, near California Route 127, in the NW1/4 sec. 27 and SW 1/4 sec. 21, T. 24 N., R. 6 E.		
Top of section; top of exposure.		
Eagle Mountain Formation (incomplete):		
44.	Sandstone, as in unit 30, beds 30 cm to 1 m thick, with chert nodules and eolian cross-bedding in top 50 cm.	18
43.	Limestone, yellowish-gray (5Y 7/2) to light gray (N7), finely laminated, chert stringers, and fine ripple laminae in silty layers to 1 cm thick.	3
42.	Pyroclastic fall, pale greenish-yellow (10Y 8/2) to moderate greenish-yellow (10Y 7/4), calcite cement, poorly exposed.	1
41.	Sandstone, as in unit 30, massive.	7
40.	Micrite, pinkish-gray (5YR 8/1), weathers brownish-black (5YR 2/1), with chert stringers.	1
39.	Sandstone, grayish-pink (5R 8/2) to white (N9), weathers dusky brown (5YR 2/2), coarse, moderately sorted, angular to subangular.	1
38.	Sandstone, as in unit 30.	7
37.	Sandstone, as in unit 34, with interbedded pale yellow-brown (10YR 6/2) pebble conglomerate. Local 2–10-cm-thick calcareous siltstone partings. Planar laminae, with soft-sediment deformation features (flame structures) near top.	6
36.	Sandstone, as in unit 30, with alternating planar and ripple laminae 5–15 cm thick.	13
35.	Sandstone as in unit 34, with ripple laminae and planar laminae as opposed to cross-bedding. One silty, calcareous layer near the base.	3
34.	Sandstone, pale yellowish-brown (10YR 6/2) to grayish-orange (10YR 7/4), poorly sorted, angular to rounded, fine to coarse, siltstone partings; bedding grades upward from low-angle cross-beds to planar laminae.	1
33.	Interbedded dark yellowish-orange (10YR 6/6) siltstone and moderate yellowish-brown (10YR 5/4) sandstone. Siltstone as in unit 32. Sandstone is fine to coarse, subangular, moderately sorted, with alternating ripple and planar laminae. Interbeds are each ~20–30 cm thick.	2
32.	Siltstone and fine sandstone, grayish-orange (10YR 7/4) to moderate yellowish-brown (10YR 5/4), calcareous.	2
31.	Siltstone, grayish-orange (10YR 7/4) to moderate yellowish-brown (10YR 5/4), calcareous, millimeter- to centimeter-scale partings.	2
30.	Sandstone, grayish-orange (10YR 7/4) to dark yellowish-orange (10YR 6/6), medium, subangular, well-sorted sand. Bed thickness ~50 cm, with weak ~1 cm planar laminae. Basal contact infills top of underlying conglomerate.	3

TABLE A1. (Continued)

Bed	Description	m
29.	Conglomerate, as in unit 26, with sandy lenses to 15 cm thick.	21
28.	Sandstone, as in unit 23, with ripple laminae in the upper 1 m.	5
27.	Sandstone, moderate reddish-brown (10R 4/6), medium, subangular to subrounded, well sorted. Includes planar lenses of conglomerate ~5 cm thick between 10–25-cm-thick sand layers.	1
26.	Conglomerate, moderate reddish-brown (10R 4/6), very coarse sand to boulders (20 cm), subangular to well rounded, and poorly sorted. Clasts consist of quartzite, limestone, and leucomonzogabbro in a matrix of fine to coarse, poorly sorted, angular to subrounded sand.	2
25.	Shale, very pale orange (10YR 8/2), calcareous, 2 mm partings. Small black spots (~1 mm) on parting surfaces.	2
24.	Sandstone, as in unit 23.	4
23.	Sandstone, moderate reddish-brown (10R 4/6), with grayish yellow-green (5GY 7/2) lenses, medium to fine, subrounded, very well sorted sand. Planar laminae present.	7
22.	Sandstone, moderate brown (5YR 4/4) to pale brown (5YR 5/2), fine to medium, subangular to subrounded grains. Well sorted in 20 cm beds, with ripple laminae and local siltstone layers.	2
21.	Sandstone, pale brown (5YR 5/2) to light brown (5YR 6/4), fine grained, angular to subrounded grains, moderately sorted. Massive base with planar laminated top, stringers of pebbles and clast-supported conglomerate.	2
20.	Mudstone, dark yellowish-orange (10YR 6/6), calcareous, includes fine sand and local rip-up clasts of mudstone.	1
19.	Sandstone, light brownish-gray (5YR 6/1), medium to fine grained, subangular to rounded, well sorted. Local stringers of subrounded to rounded pebbles and cobbles, blocky weathering pattern.	5
18.	Sandstone, light brown (5YR 6/4) angular to subrounded grains, poorly sorted, planar bedding with some low-angle cross-bedding.	4
17.	Conglomerate, moderate reddish-brown (10R 4/6), pebble- to boulder-sized clasts (15 cm), typically subrounded and poorly sorted. Clast supported, with clasts of dolostone, limestone, and quartzite. Matrix consists of moderate brown (5YR 4/4) fine to very coarse, angular to subrounded sand.	2
16.	Sandstone, light brownish-gray, (5YR 6/1), fine to medium grained, subangular to subrounded grains, moderately sorted, with rare fine mudstone laminae.	2
15.	Sandstone, very pale orange (10YR 8/2), very fine grained, moderately well sorted, with 0.5–1 cm partings.	1
14.	Sandstone, light brown (5YR 6/4), medium to fine grained. Upper 40 cm weathers moderate reddish-brown (10R 4/6). Angular to subrounded grains, moderately well sorted. Calcite cement, cross-bedded, reduction spots common.	1
13.	Sandstone, brownish-gray (5YR 4/1), medium grained, with angular to subrounded grains. Moderately sorted, massive, with calcite cement.	4
12.	Conglomerate, as described in unit 11, clast supported.	5
11.	Sandstone, moderate brown (5YR 4/4), coarse, angular to subrounded, poorly sorted, with local subangular pebbles and cobbles of dolostone, limestone, and quartzite. Calcite cemented.	3
10.	Sandstone, moderate brown (5YR 4/4) to moderate reddish-brown (10R 4/6), medium to fine grained, subangular to moderately rounded grains, moderately well sorted. Beds 30 cm to 1 m thick, calcite cement. Interbedded lenses and	19

TABLE A1. (Continued)

Bed	Description	m
	layers of conglomerate to 20 cm thick of subangular to well-rounded, coarse sand to pebble-sized clasts including dolostone, quartzite, and calcareous mudstone, matrix supported.	
9.	Siltstone and mudstone, light brown (5YR 6/4), planar laminae with 2 mm to 1 cm shaly partings. Interbedded conglomerate and sandstone.	4
8.	Mudstone to fine-grained sandstone, pale red-purple (5RP 6/2) to pale blue (5PB 7/2), bedding thickness 20 cm to 1 m, calcareous, shows soft-sediment deformation where loaded by overlying conglomerates.	2
7.	Covered interval.	1
6.	Mudstone, very pale orange (10YR 8/2), calcareous, with millimeter-scale laminae. Interbedded conglomerates as described in unit 2. Soft-sediment deformation is present.	3
5.	Covered interval.	3
4.	Siltstone and very fine sandstone, as in unit 3.	5
3.	Siltstone, moderate reddish-orange (10R 6/6) to light brown (5YR 5/6), calcareous, planar laminated, with interbedded conglomerates as described in unit 2. Interbedded pyroclastic falls, white (N9), fine grained, silicified, to 30 cm thick.	2
2.	Conglomerate, light to dark gray clasts (N7–N3) in a light brown (5YR 5/6) matrix, clast size from coarse sand to ~15 cm, angular to subrounded clasts, poorly sorted, dolostone clasts in a calcareous mudstone matrix, matrix supported at base, clast supported near top, calcite cement, clasts at top of unit overgrown by algal laminae.	1
1.	Conglomeratic breccia, medium gray (N5) to grayish-black (N2), with clasts of Bonanza King, pebble to boulder sized, angular clasts, poorly sorted, clast supported, no visible bedding, with intercalated tephra.	106
Total, incomplete Eagle Mountain Formation	Base of section, unconformable on Cambrian Bonanza King Formation	291

Note: m = thickness in meters. See Figure 3. Measured by R.J. Brady and N.A. Niemi, June 1995.

TABLE A2. RESTING SPRING RANGE SOUTHERN SECTION

Bed	Description	m
Eastern side of the Resting Spring Range, California, measured parallel to the Baxter Mine Road, SW1/4 sec. 9, T. 23 N., R. 7 E.		
Top of section; top of exposure.		
Eagle Mountain Formation—Lower (incomplete):		
4.	Conglomerate, as in unit 1, except matrix weathers mainly yellow (5Y 5/8), poorly stratified; fault contact at base.	70
3.	Pyroclastic fall, pale greenish-yellow (10Y 8/2) to yellowish-gray (5Y 7/2) or white (N9); weathers same color. Highly friable, altered and reworked.	8
2.	Conglomerate, as in unit 1, mainly pebbles. Weathers pale greenish-yellow (10Y 8/2) with matrix rich in volcanic ash.	8
1.	Conglomerate, weathers moderate orange-pink (10R 7/4), subangular to rounded, moderately to very poorly sorted, crudely stratified, clasts of orthoquartzite, limestone, and sandstone, to 70 cm in diameter. Clast supported with a matrix of sand.	54
Total, incomplete Eagle Mountain Formation	Base of section; unconformable on Cambrian Zabriskie Quartzite	140

Note: m = thickness in meters. See Figure 5. Measured by B.P. Wernicke, April 1993.

TABLE A3. RESTING SPRING RANGE NORTHERN SECTION

Bed	Description	m
Eastern side of the Resting Spring Range, California, measured in the NE1/2 sec. 2, T. 23 N., R. 7 E.		
Top of section; top of exposure.		
Eagle Mountain Formation (incomplete):		
25.	Conglomerate, as in unit 11, with boulders to 60 cm.	4
24.	Pyroclastic fall, pale greenish-yellow (10Y 8/2), light gray (N7) and white weathering, altered and reworked, friable.	11
23.	Sandstone, as in unit 1, with pebbly to cobbly bed near center of unit.	5
22.	Conglomerate, as in unit 11.	1
21.	Sandstone, as in units 1 and 3.	11
20.	Pyroclastic fall, pinkish-gray (5YR 8/1), white to very light gray (N8) weathering, reworked top, well indurated.	2
19.	Sandstone, as in unit 1, locally granular or pebbly.	3
18.	Siltstone, poorly exposed, pale greenish-yellow (10Y 8/2) weathering surfaces.	2
17.	Sandstone and siltstone, thin to medium bedded, friable with ashy matrix, as in portions of unit 1; silty intervals mainly covered.	5
16.	Sandstone, as in unit 1. Well-developed cross-bedding with foreset packages to 50 cm thick dipping 25° with respect to surrounding bedding.	2
15.	Conglomerate, with small cobbles and boulders, fining upward into pebbly sand as in unit 1.	2
14.	Sandstone, as in units 1 and 3, with a few thin-bedded silty horizons.	6
13.	Conglomerate and sandstone. Boulders generally finer than in unit 11, to 30 cm maximum dimension, conglomerate fines upward to pebbly sand similar to units 1 and 3.	3
12.	Sandstone, as in units 1 and 3. Locally pebbly.	3
11.	Conglomerate, rounded to well-rounded clasts, typically 30–70 cm in diameter, moderately to very poorly sorted, crudely stratified, with one clast (not in place) >1 m in diameter.	5
10.	Pebbly sandstone, as at base of unit 1.	3
9.	Sandstone as in units 1 and 3.	5
8.	Sandstone, as in unit 2, siltstone, and pebbly sandstone as in units 1 and 3.	2
7.	Sandstone as in units 1 and 3.	4
6.	Pyroclastic fall, pale yellowish-brown (10YR 6/2), weathers grayish-orange (10YR 7/4) to pale yellowish-orange (10YR 8/6), crystal rich with quartz, sanidine, and altered mafic minerals, reworked with probable detrital minerals.	1
5.	Sandstone, as in units 1 and 3.	5
4.	Pyroclastic fall, pale olive (10Y 6/2) to pale greenish-yellow (10Y 8/2), pale yellowish-orange (10YR 8/6) weathering, possibly reworked.	1
3.	Sandstone, grayish-yellow (5Y 8/4) and dusky yellow (5Y 6/4) on fresh surfaces, weathers same color or grayish-orange (10YR 7/4). Medium to coarse grained, subrounded to rounded grains, well sorted. Friable, weakly indurated, with ashy matrix, not as dense as unit 2.	13
2.	Pebbly sandstone, pale yellowish-brown (10YR 6/2) to dusky yellow (5Y 6/4), weathers grayish-orange (10YR 7/4). Medium grained to granular with pebbles to 5 cm maximum dimension, moderately to well sorted. Well indurated and resistant compared with surrounding units.	3

TABLE A3. (Continued)

Bed	Description	m
1.	Sandstone, grayish-yellow (5Y 8/4) to pale greenish-yellow (10Y 8/2), weathers grayish-orange (10YR 7/4). Medium grained to granular, moderately to well sorted. Basal conglomerate contains subangular to subrounded clasts of underlying material, to 8 cm in maximum dimension. Locally ashy matrix. Moderate to weak induration. Generally parallel bedded with local cross-bedding in packages about 10–20 cm thick.	9
Total, incomplete Eagle Mountain Formation	Base of section, unconformable on Cambrian Carrara Formation and Zabriskie Quartzite	101

Note: m = thickness in meters. See Figure 3. Measured by B.P. Wernicke, April 1993.

APPENDIX 2. ANALYTICAL METHODS

⁴⁰Ar/³⁹Ar Geochronology

Sanidine was separated by standard magnetic and density methods and then hand-picked for maximum purity. The purity of separates was verified by electron probe microanalysis of representative grains mounted in epoxy using the JEOL 733 electron microprobe at the California Institute of Technology (Tables DR4, DR7, and DR10; see footnote 1). Separates were washed in water, acetone, and ethanol prior to packaging in individual aluminum foil packets for irradiation.

Separates were irradiated at the McMaster University reactor facility with Cd shielding. Corrections for interfering reactions on Ca, K, and Cl were based on analyses of CaF₂, K₂SO₄, and KCl included in the irradiation package. Fast neutron flux was monitored by using FC-1 sanidine from the Fish Canyon Tuff (27.84 Ma for samples analyzed prior to January 1996, including 1893A and 1893B, Cebula et al., 1986; 27.95 Ma for samples analyzed after January 1996, including EM-0, EM-4, 1593, B. Olszewski, 1997, oral commun.).

Irradiated samples were analyzed at the Cambridge Laboratory for Argon Isotopic Research (CLAIR) at the Massachusetts Institute of Technology by both laser-fusion and resistance-furnace gas extraction systems coupled to a MAP 215–50 mass spectrometer. Laboratory procedures are discussed in Hodges et al. (1994).

U/Pb Geochronology

Baddeleyite was separated from ~15 kg of crushate by standard density and magnetic separation techniques. Dissolution and chemical extraction was performed at the California Institute of Technology using techniques similar to those described by Krogh (1973). Mass spectrometry was performed on a VG Sector multicollector instrument at the California Institute of Technology. Pb and U were run on outgassed Re single filaments with silica gel and graphite loads, respectively. A more detailed discussion of laboratory procedures is presented in Saleeby et al. (1989).

ACKNOWLEDGMENTS

This research was supported by National Science Foundation (NSF) grants EAR-93-16797 and EAR-

96–14780 (to Wernicke), EAR-95–26859 (to Saleeby), and an NSF Graduate Fellowship (to Niemi). Discussions and field excursions with S. Beard, R. Bohannon, J. Calzia, I. Cemen, H.D. Curry, K. Fowler, C.J. Friedrich, J. Friedmann, W. Hamilton, K.V. Hodges, M.R. McMackin, T.L. Pavlis, A.R. Prave, P. Ryder, J.K. Snow, L. Serpa, L.T. Silver, C.H. Stevens, D.J. Topping, B.W. Troxel, J.D. Walker, and L.A. Wright have contributed to the ideas presented here, but they are in no way liable for any errors in fact and interpretation. We thank Neil A. Niemi and J.A. Grover for field assistance and J.K. Snow, D.L. Lux, and L.A. Wright for providing copies of their manuscripts prior to publication. Constructive reviews by W. Taylor and an anonymous reader greatly improved the clarity and presentation of this manuscript. Stereonet and MacStrat by R.W. Allmendinger were used for the analysis and plotting of data.

REFERENCES CITED

- Abolins, M.A., 1998, I. Stratigraphic constraints on the number of discrete Neoproterozoic glaciations and the relationship between glaciation and ediacaran evolution; and II. The Kwichup Spring thrust in the northwestern Spring Mountains, Nevada: Implications for large-magnitude extension and the structure of the Cordilleran thrust belt [Ph.D. dissert.]: Pasadena, California Institute of Technology, 348 p.
- Anstey, R.L., 1965, Physical characteristics of alluvial fans: Natick, Massachusetts, Natick Laboratory Army Research, Development, and Engineering Center, U.S. Army Cold Regions Research and Engineering Laboratory Technical Report ES-20, 109 p.
- Anstey, R.L., 1966, A comparison of alluvial fans in west Pakistan and the United States: *Pakistan Geographical Review*, v. 21, p. 14–20.
- Atwater, T., and Stock, J.M., 1998, Pacific-North America plate tectonics of the Neogene southwestern United States: An update: *International Geological Review*, v. 40, p. 375–402.
- Axen, G.J., and Bartley, J.M., 1997, Field-tests of rolling hinges: Existence, mechanical types, and implications for extensional tectonics: *Journal of Geophysical Research*, v. 102, p. 20515–20537.
- Bachman, G.O., and Mehnert, H.H., 1978, New K-Ar dates and the late Pliocene to Holocene geomorphic history of the central Rio Grande region, New Mexico: *Geological Society of America Bulletin*, v. 89, p. 283–292.
- Beaty, C.B., 1989, Great big boulders I have known: *Geology*, v. 17, p. 349–352.
- Bennett, R.A., Wernicke, B.P., Davis, J.L., Elósegui, P., Snow, J.K., Abolins, M.J., House, M.A., Stirewalt, G.L., and Ferrill, D.A., 1997, Global positioning system constraints on fault slip rates in the Death Valley region, California and Nevada: *Geophysical Research Letters*, v. 24, p. 3073–3076.
- Blair, T.C., 1987, Sedimentary processes, vertical stratification sequences, and geomorphology of the Roaring River alluvial fan, Rocky Mountain National Park, Colorado: *Journal of Sedimentary Petrology*, v. 57, p. 1–18.
- Blair, T.C., and McPherson, J.G., 1994, Alluvial fans and their natural distinction from rivers based on morphology, hydraulic processes, sedimentary processes, and facies assemblages: *Journal of Sedimentary Research*, v. A64, p. 450–489.
- Brierley, G.J., Liu, K., and Crook, K.A.W., 1993, Sedimentology of coarse-grained alluvial fans in the Markham Valley, Papua New Guinea: *Sedimentary Geology*, v. 86, p. 297–324.
- Buck, W.R., 1988, Flexural rotation of normal faults: *Tectonics*, v. 7, p. 959–973.
- Burchfiel, B.C., Pelton, P.J., and Sutter, J., 1970, An early Mesozoic deformation belt in south-central Nevada-southeastern California: *Geological Society of America Bulletin*, v. 81, p. 211–215.
- Burchfiel, B.C., Hamill, G.S., and Wilhelms, D.E., 1982, Stratigraphy of the Montgomery Mountains and the northern half of the Nopah and Resting Spring Ranges, Nevada and California: *Geological Society of America Map and Chart Series MC44*, scale 1:62 500, 9 p.
- Burchfiel, B.C., Hamill, G.S., and Wilhelms, D.E., 1983, Structural geology of the Montgomery Mountains and the northern half of the Nopah and Resting Spring Ranges, Nevada and California: *Geological Society of America Bulletin*, v. 94, p. 1359–1376.
- Byers, F.M., Jr., Carr, W.J., Christiansen, R.L., Lipman, P.W., Orkild, P.P., and Quinlivan, W.D., 1976, Geologic map of the Timber Mountain caldera area, Nye County, Nevada: U.S. Geological Survey Miscellaneous Investigations Map I-0891, scale 1:48 000, 10 p.
- Cebula, G.T., Kunk, M.J., Mehnert, H.H., Naeser, C.W., Obradovich, J.D., and Sutter, J.F., 1986, The Fish Canyon Tuff, a potential standard for the ^{40}Ar – ^{39}Ar and fission-track methods: *Terra Cognita*, v. 6, p. 139–140.
- Cemen, I., and Wright, L.A., 1988, Stratigraphy and chronology of the Artist Drive Formation, Furnace Creek Basin, Death Valley, California, in Gregory, J.L., and Baldwin, E.J., eds., *Geology of the Death Valley region: Santa Ana, California*, South Coast Geological Society, Field Trip Guidebook 16, p. 77–87.
- Cemen, I., Wright, L.A., Drake, R.E., and Johnson, F.C., 1985, Cenozoic sedimentation and sequence of deformational events at the southeastern end of the Furnace Creek strike-slip fault zone, Death Valley region, California, in Biddle, K.T., and Christie-Blick, N., eds., *Strike-slip deformation, basin formation, and sedimentation: Society of Economic Paleontologists and Mineralogists Special Publication 37*, p. 127–141.
- Cemen, I., Wright, L.A., and Prave, A.R., 1999, Stratigraphy and tectonic implications of the latest Oligocene and early Miocene sedimentary succession, southernmost Funeral Mountains, Death Valley region, California, in Wright, L.A., and Troxel, B.W., eds., *Cenozoic basins of the Death Valley region: Geological Society of America Special Paper 333*, p. 65–86.
- Chen, J.H., and Tilton, G., 1991, Applications of lead and strontium isotopic relationships to the petrogenesis of granitoid rocks, central Sierra-Nevada batholith, California: *Geological Society of America Bulletin*, v. 103, p. 439–447.
- Chen, J.H., and Wasserburg, G.J., 1981, Isotopic determination of uranium in picomole and subpicomole quantities: *Analytical Chemistry*, v. 53, p. 2060–2067.
- Corbett, K.P., 1990, Basin and Range extensional tectonics at the latitude of Las Vegas, Nevada: Discussion: *Geological Society of America Bulletin*, v. 102, p. 267–268.
- Davis, G.A., Fowler, T.K., Bishop, K.M., Brudos, T.C., Friedmann, S.J., Burbank, D.W., Parke, M.A., and Burchfiel, B.C., 1993, Pluton pinning of an active Miocene detachment fault system, eastern Mojave Desert, California: *Geology*, v. 21, p. 627–630.
- DeCelles, P.G., Langford, R.P., and Schwartz, R.K., 1983, Two new methods of paleocurrent determination from trough cross-stratification: *Journal of Sedimentary Petrology*, v. 53, p. 629–642.
- Denny, C.S., 1965, Alluvial fans in the Death Valley region, California and Nevada: U.S. Geological Survey Professional Paper 466, 62 p.
- Dickinson, W.R., and Wernicke, B.P., 1997, Reconciliation of San Andreas slip discrepancy by a combination of interior Basin and Range extension and transrotation near the coast: *Geology*, v. 27, p. 663–665.
- Dorsey, R.J., and Roberts, P., 1996, Evolution of the Miocene north Whipple basin in the Aubrey Hills, western Arizona, upper plate of the Whipple detachment fault, in Beratan, K.K., ed., *Reconstructing the history of Basin and Range extension using sedimentology and stratigraphy: Geological Society of America Special Paper 303*, p. 127–146.
- Fowler, T.K., and Calzia, J.P., 1999, Kingston Range detachment fault, southeastern Death Valley region, California: Relation to Tertiary deposits and reconstruction of initial dip, in Wright, L.A., and Troxel, B.W., eds., *Cenozoic basins of the Death Valley region: Geological Society of America Special Paper 333*, p. 245–257.
- Fowler, T.K., Friedmann, S.J., Davis, G.A., and Bishop, K.M., 1995, 2-phase evolution of the Shadow Valley basin, south-eastern California: A possible record of footwall uplift during extensional detachment faulting: *Basin Research*, v. 7, p. 165–179.
- Friedmann, S.J., 1999, Sedimentology and stratigraphy of the Shadow Valley basin, eastern Mojave Desert, California, in Wright, L.A., and Troxel, B.W., eds., *Cenozoic basins of the Death Valley region: Geological Society of America Special Paper 333*, p. 213–243.
- Friedmann, S.J., and Burbank, D.W., 1995, Rift basins and supradetachment basins: Intracontinental extensional end-members: *Basin Research*, v. 7, p. 109–127.
- Frizzell, V.A., Jr., and Shulters, J.C., 1990, Geologic map of the Nevada Test Site, southern Nevada: U.S. Geological Survey Miscellaneous Investigations Series Map I-2046, scale 1: 100 000.
- Greene, R.C., 1997, Geology of the northern Black Mountains, Death Valley, California: U.S. Geological Survey Open-File Report 97–79, 110 p.
- Hamilton, W.B., 1988, Death Valley tectonics; hingeline between active and inactivated parts of a rising and flattening master normal fault, in Gregory, J.L., and Baldwin, E.J., eds., *Geology of the Death Valley region: Santa Ana, California*, South Coast Geological Society, Field Trip Guidebook 16, p. 179–205.
- Hand, B.M., Wessel, J.M., and Hayes, M.O., 1969, Antidunes in the Mount Toby Conglomerate (Triassic), Massachusetts: *Journal of Sedimentary Petrology*, v. 39, p. 1310–1316.
- Hodges, K.V., McKenna, L.W., Stock, J., Knapp, J., Page, L., Sternlof, K., Silverberg, D., Wust, G., and Walker, J.D., 1989, Evolution of extensional basins and Basin and Range topography west of Death Valley, California: *Tectonics*, v. 8, p. 453–467.
- Hodges, K.V., Hames, W.E., Olszewski, W.J., Burchfiel, B.C., Royden, L.H., and Chen, Z., 1994, Thermobarometric and $^{40}\text{Ar}/^{39}\text{Ar}$ geochronologic constraints on Eohimalayan metamorphism in southern Tibet: Contributions to Mineralogy and Petrology, v. 117, p. 151–163.
- Hoisch, T.D., Heizler, M.T., and Zartman, R.E., 1997, Timing of detachment faulting in the Bullfrog Hills and Bare Mountain area, southwest Nevada; inferences from $^{40}\text{Ar}/^{39}\text{Ar}$, K-Ar, U-Pb, and fission track thermochronology: *Journal of Geophysical Research*, v. 102, p. 2815–2833.
- Holm, D.K., and Dokka, R.K., 1993, Interpretation and tectonic implications of cooling histories: An example from the Black Mountains, Death Valley extended terrane, California: *Earth and Planetary Science Letters*, v. 116, p. 63–80.
- Holm, D.K., and Wernicke, B.P., 1990, Black Mountains crustal section, Death Valley extended terrain, California: *Geology*, v. 18, p. 520–523.
- Holm, D.K., Snow, J.K., and Lux, D.R., 1992, Thermal and barometric constraints on the intrusive and unroofing history of the Black Mountains: Implications for timing, initial dip, and kinematics of detachment faulting in the Death Valley region, California: *Tectonics*, v. 11, p. 507–522.
- Holm, D.K., Fleck, R.J., and Lux, D.R., 1994, The Death Valley turtlebacks reinterpreted as Miocene-Pliocene folds of a major detachment surface: *Journal of Geology*, v. 102, p. 718–727.
- Jaffey, A.H., Flynn, K.F., Glendenin, L.E., Bentley, W.C., and Essling, A.M., 1971, Precision measurement of half-lives and specific activities of ^{235}U and ^{238}U : *Physics Reviews*, v. C4, p. 1889–1906.
- Jopling, A.V., and Richardson, E.V., 1966, Backset bedding developed in shooting flow in laboratory experiments: *Journal of Sedimentary Petrology*, v. 36, p. 821–824.
- Krogh, T.E., 1973, A low-contamination method for hydrothermal decomposition of zircon and extraction of U and Pb for isotopic age determinations: *Geochimica et Cosmochimica Acta*, v. 37, p. 485–494.
- Kruse, S., McNutt, M.L., Phipps-Morgan, J., Royden, L., and Wernicke, B., 1991, Lithospheric extension near Lake Mead, Nevada: A model for ductile flow in the lower crust: *Journal of Geophysical Research*, v. 96, p. 4435–4456.
- Leeder, M.R., and Gawthorpe, R.L., 1987, Sedimentary

- models for extensional tilt-block/half-graben basins, *in* Coward, M.P., et al., eds., *Continental extensional tectonics: Geological Society [London] Special Publication 28*, p. 139–152.
- Mancktelow, N.S., and Pavlis, T.L., 1994, Fold-fault relationships in low-angle detachment systems: *Tectonics*, v. 13, p. 668–685.
- McAllister, J.F., 1970, Geology of the Furnace Creek borate area, Death Valley, Inyo County, California: California Division of Mines and Geology Map Sheet 14, scale 1:24 000, 9 p.
- McAllister, J.F., 1973, Geologic map and sections of the Amargosa Valley borate area—Southeast continuation of the Furnace Creek area—Inyo County, California: U.S. Geological Survey Miscellaneous Investigations Series Map I-782, scale 1:24 000.
- McDougall, I., and Harrison, T.M., 1988, Geochronology and thermochronology by the $^{40}\text{Ar}/^{39}\text{Ar}$ method: New York, Oxford University Press, 212 p.
- McKenna, L.W., and Hodges, K.V., 1990, Constraints on kinematics and timing of late Miocene–recent extension between Panamint and Black Mountains, southeastern California, in Wernicke, B.P., ed., *Basin and Range extensional tectonics near the latitude of Las Vegas, Nevada: Geological Society of America Memoir 176*, p. 363–376.
- Middleton, G.V., 1965, Antidune cross-bedding in a large flume: *Journal of Sedimentary Petrology*, v. 35, p. 922–927.
- Power, W.R., Jr., 1961, Backset beds in the Coso Formation, Inyo County, California: *Journal of Sedimentary Petrology*, v. 31, p. 603–607.
- Prave, A.R., and Wright, L.A., 1986, Isopach pattern of the Lower Cambrian Zabriskie Quartzite, Death Valley region, California-Nevada: How useful in tectonic reconstruction? *Geology*, v. 14, p. 251–254.
- Reynolds, S.J., and Spencer, J.E., 1985, Evidence for large-scale transport on the Bullard detachment fault, west-central Arizona: *Geology*, v. 13, p. 353–356.
- Rowland, S.M., Parolini, J.R., Eschner, E., and McAllister, A.J., 1990, Sedimentologic and stratigraphic constraints on the Neogene translation and rotation of the Frenchman Mountain structural block, Clark County, Nevada, *in* Wernicke, B.P., ed., *Basin and Range extensional tectonics near the latitude of Las Vegas, Nevada: Geological Society of America Memoir 176*, p. 99–122.
- Rust, B.R., and Koster, E.H., 1984, Coarse alluvial deposits, *in* Walker, R.G., ed., *Facies models (second edition)*: Toronto, Geological Association of Canada, p. 53–70.
- Saleeby, J.B., and Busby-Spera, C., 1992, Early Mesozoic tectonic evolution of the western U.S. Cordillera, *in* Burchfiel, B.C., et al., eds., *The Cordilleran orogen: Conterminous U.S.: Boulder, Colorado, Geological Society of America, Geology of North America*, v. G-3, p. 107–168.
- Saleeby, J.B., Geary, E.E., Paterson, S.R., and Tobisch, O.T., 1989, Isotopic systematics of Pb/U (zircon) and $^{40}\text{Ar}/^{39}\text{Ar}$ (biotite-hornblende) from rocks of the central Foothills terrane, Sierra Nevada, California: *Geological Society of America Bulletin*, v. 101, p. 1481–1492.
- Sawyer, D.A., Fleck, R.J., Lanphere, M.A., Warren, R.G., Broxton, D.E., and Hudson, M.R., 1994, Episodic caldera volcanism in the Miocene southwestern Nevada volcanic field; revised stratigraphic framework, $^{40}\text{Ar}/^{39}\text{Ar}$ geochronology, and implications for magmatism and extension: *Geological Society of America Bulletin*, v. 106, p. 1304–1318.
- Serpa, L., and Pavlis, T.L., 1996, Three-dimensional model of the late Cenozoic history of the Death Valley region, southeastern California: *Tectonics*, v. 15, p. 1113–1128.
- Smith, G.A., 1987, Sedimentology of volcanism-induced aggradation in fluvial basins; examples from the Pacific Northwest, U.S.A., *in* Ethridge, F.G., et al., eds., *Recent developments in fluvial sedimentology: Society of Economic Paleontologists and Mineralogists Special Publication 39*, p. 217–228.
- Snow, J.K., 1992, Large-magnitude Permian shortening and continental margin tectonics in the southern Cordillera: *Geological Society of America Bulletin*, v. 104, p. 80–105.
- Snow, J.K., and Lux, D.R., 1999, Tectono-sequence stratigraphy of Tertiary rocks in the Cottonwood Mountains and northern Death Valley area, California and Nevada, *in* Wright, L.A., and Troxel, B.W., eds., *Cenozoic basins of the Death Valley region: Geological Society of America Special Paper 333*, p. 17–64.
- Snow, J.K., and Prave, A.R., 1994, Covariance of structural and stratigraphic trends: Evidence for anticlockwise rotation within the Walker Lane belt, Death Valley region, California and Nevada: *Tectonics*, v. 13, p. 712–724.
- Snow, J.K., and Wernicke, B., 1989, Uniqueness of geological reconstructions: An example from the Death Valley extended terrain: *Geological Society of America Bulletin*, v. 101, p. 1351–1362.
- Stevens, C.H., Stone, P., and Belasky, P., 1991, Paleogeographic and structural significance of an Upper Mississippian facies boundary in southern Nevada and east-central California: *Geological Society of America Bulletin*, v. 103, p. 876–885.
- Stevens, C.H., Stone, P., and Belasky, P., 1992, Paleogeographic and structural significance of an Upper Mississippian facies boundary in southern Nevada and east-central California: Reply: *Geological Society of America Bulletin*, v. 104, p. 1067–1069.
- Stewart, J.H., 1970, Upper Precambrian and Lower Cambrian strata in the southern Great Basin, California and Nevada: U.S. Geological Survey Professional Paper 620, 206 p.
- Stewart, J.H., 1983, Extensional tectonics in the Death Valley area, California: Transport of the Panamint Range structural block 80 km northwestward: *Geology*, v. 11, p. 153–157.
- Stone, P., and Stevens, C.H., 1993, Large-magnitude Permian shortening and continental-margin tectonics in the southern Cordillera: Discussion: *Geological Society of America Bulletin*, v. 105, p. 279–280.
- Tera, F., and Wasserburg, G.J., 1972, U-Th-Pb systematics in three Apollo 14 basalts and the problem of initial Pb in lunar rocks: *Earth and Planetary Science Letters*, v. 14, p. 281–304.
- Topping, D.J., 1993, Paleogeographic reconstruction of the Death Valley extended region: Evidence from Miocene large rock-avalanche deposits in the Amargosa Chaos Basin, California: *Geological Society of America Bulletin*, v. 105, p. 1190–1213.
- Troxel, B.W., 1989, Geologic road guide: Day 2—Segment 3—Shoshone to eastern Funeral range, *in* Cooper, J.D., ed., *Cavalcade of carbonates: American Association of Petroleum Geologists and Society of Economic and Petroleum Geologists Guidebook, Field trip 3*, p. 14–20.
- Wdowinski, S., and Axen, G.J., 1992, Isostatic rebound due to tectonic denudation: A viscous flow model of a layered lithosphere: *Tectonics*, v. 11, p. 303–315.
- Wernicke, B., 1992, Cenozoic extensional tectonics of the U.S. Cordillera, *in* Burchfiel, B.C., et al., eds., *The Cordilleran orogen: Conterminous U.S.: Boulder, Colorado, Geological Society of America, Geology of North America*, v. G-3, p. 553–581.
- Wernicke, B., and Axen, G.J., 1988, On the role of isostasy in the evolution of normal fault systems: *Geology*, v. 16, p. 848–851.
- Wernicke, B., and Burchfiel, B.C., 1982, Modes of extensional tectonics: *Journal of Structural Geology*, v. 4, p. 105–115.
- Wernicke, B., and Snow, J.K., 1998, Cenozoic tectonism in the central Basin and Range: motion of the Sierran—Great Valley block: *International Geology Review*, v. 40, p. 403–410.
- Wernicke, B., Axen, G.J., and Snow, J.K., 1988, Basin and Range extensional tectonics at the latitude of Las Vegas, Nevada: *Geological Society of America Bulletin*, v. 100, p. 1738–1757.
- Wernicke, B., Snow, J.K., Hodges, K.V., and Walker, J.D., 1993, Structural constraints on Neogene tectonism in the southern Great Basin, *in* Lahren, M.M., et al., eds., *Crustal evolution of the Great Basin and the Sierra Nevada: Cordilleran/Rocky Mountain Section, Geological Society of America Guidebook: Reno, University of Nevada, Department of Geological Sciences*, p. 453–479.
- Wilhelms, D.E., 1962, Geology of part of the Nopah and Resting Spring Ranges, Inyo County, California [Ph.D. dissert.]: Los Angeles, University of California, 224 p.
- Wright, L.A., Thompson, R.A., Troxel, B.W., Pavlis, T.L., DeWitt, E.H., Otton, J.K., Ellis, M.A., Miller, M.G., and Serpa, L.F., 1991, Cenozoic magmatic and tectonic evolution of the east-central Death Valley region, California, *in* Walawender, M.J., and Hanan, B.B., eds., *Geological excursions in southern California and Mexico: Annual Meeting, Geological Society of America Guidebook, San Diego, California, San Diego State University, Department of Geological Sciences*, p. 93–127.
- Wright, L.A., Greene, R.C., Cemen, I., Johnson, F.C., and Prave, A.R., 1999, Tectonostratigraphic development of the Miocene-Pliocene Furnace Creek Basin, and related features, Death Valley region, California, *in* Wright, L.A., and Troxel, B.W., eds., *Cenozoic basins of the Death Valley region: Geological Society of America Special Paper 333*, p. 87–114.
- York, D., 1969, Least-squares fitting of a straight line with correlated errors: *Earth and Planetary Science Letters*, v. 5, p. 320–324.

MANUSCRIPT RECEIVED BY THE SOCIETY MARCH 30, 2000

MANUSCRIPT ACCEPTED APRIL 19, 2000

Printed in the USA